Mechanical backreaction effect of the dynamical Casimir emission

Salvatore Butera and Iacopo Carusotto
INO-CNR BEC Center and Dipartimento di Fisica, Università di Trento, I-38123 Povo, Italy

(Received 26 October 2018; published 13 May 2019)

We consider an optical cavity enclosed by a freely moving mirror attached to a spring and we study the quantum friction effect exerted by the dynamical Casimir emission on the mechanical motion of the mirror. Observable signatures of this simplest example of backreaction effect are studied in both the ring-down oscillations of the mirror motion and in its steady-state motion under a monochromatic force. Analytical expressions are found in simple yet relevant cases and compared to complete numerical solution of the master equation. In order to overcome the experimental difficulties posed by the weakness of the backreaction effect in current setups, a promising circuit-QED device allowing for the observation of an analog backreaction effect with state-of-the-art technology is proposed and theoretically characterized.

DOI: 10.1103/PhysRevA.99.053815

I. INTRODUCTION

The rich physics of quantum fields living on curved spacetimes and/or subject to boundary conditions has been an active field of research for a few decades [1], leading to fascinating predictions such as the Hawking radiation from black holes [2], cosmological particle creation in an expanding universe [3,4], and dynamical Casimir emission (DCE) in the presence of moving mirrors [5–7]. All these works are based on the so-called semiclassical approximation, according to which the quantum field lives on a fixed background, whose geometry and dynamics are not affected by the one of the quantum field itself.

The formulation of a complete theory that is able to take into account the backreaction of the quantum field on the background spacetime and/or on the boundary conditions is still a challenging but very rewarding problem: the anticipated observable consequences of the backreaction range in fact from the damping of the expansion of the universe by the cosmological particle creation [8–18], to the long-time evaporation of black holes [19–24], to the mechanical friction felt by the moving mirror in the DCE [25]. Given the complexity of the problem, a widespread assumption is that the background interacts with expectation values of quantum field observables such as the stress-energy tensor. Further investigations are therefore needed to get a clear picture of the quantum correlations that may appear between the field and the background beyond such an approximation, and then of their consequences on the backreaction effect [26–29].

In this work we focus on the backreaction effect of the DCE onto the motion of a moving mirror. In order to focus on the fundamental physical processes, we concentrate on the simplest formulation of the problem in terms of a single-mode cavity enclosed by massive mechanically moving mirrors. Their mutual optomechanical coupling occurs via the radiation pressure effect. The DCE consists of the conversion of quanta of mechanical motion into pairs of cavity photons [30,31], which then exert a backreaction effect on the mirror in the form of a mechanical friction [25,32]. As we will see in Secs. II–IV of the present article, unambiguous signatures of the backreaction effect are anticipated to appear in our configuration both in the relaxation dynamics of the mirror motion and in the steady state under a monochromatic mechanical drive.

In spite of the clarity of the predicted signatures of backreaction, the road towards their experimental observation is still quite long. Whereas impressive recent advances have been made in the field of quantum optomechanics [33], the conversion of the quantum fluctuations of the electromagnetic field into real photons by the mechanically moving mirrors (and, *a fortiori*, the mechanical backreaction effect) has so far escaped experimental observation [6,7]. One of the main difficulties stems from the wide separation in frequency of the (high-frequency) optical and (low-frequency) mechanical modes in standard optomechanical devices, which hinders fulfillment of the DCE resonance condition $\omega_b \approx 2\omega_a$ between the cavity and mechanical frequencies $\omega_{a,b}$ and thus dramatically suppresses the intensity of the DCE emission. While strong efforts are devoted to the development of high frequency mechanical resonators up to the GHz range [34–36], more sophisticated schemes to reinforce the DCE emission are being theoretically explored. For instance, the use of higher-harmonic couplings was proposed to release the resonant condition to $n_b\omega_b = 2\omega_a$ (n_b being an integer) [7], but the efficiency of the resulting DCE remains quite low. Very recently, a dramatically reinforced efficiency in strongly nonlinear ultrastrong light-matter coupling regimes was predicted in [37], where an investigation of the backreaction effect of DCE onto the mirror was also reported. A scheme based on an optomechanical system with a parametrically driven squeezed cavity mode was proposed in [38].

A conceptually different strategy to tackle general questions about quantum fields on curved spacetimes was pioneered by Unruh's proposal of analog Hawking radiation from sonic horizons [39]. In the rich literature that has followed, the general concept of an *analog model* turned out to be a fruitful framework to study physical phenomena whose experimental investigation is out of current technological capabilities or to

perform systematic explorations of effects that are normally observed only in uncontrolled astrophysical environments. The basic idea is to look for an experimentally controllable system, whose dynamics is governed by the same equations of motion of the system of interest, yet in a different physical context and on completely different scales. Even though much literature on analog models has followed the original work [39] and focused on the analog Hawking radiation [40–43], significant attention has also been devoted to other questions related to the quantum vacuum, in particular to analogs of the DCE. Beyond optical cavities [44–46] and atomic Bose-Einstein condensates [47–49], circuit-QED devices turned out to be one of the most fruitful platforms in this adventure [50–53].

One of the first experimental successes of the analog model idea was in fact the demonstration of DCE in a circuit-QED context [54]. Following the theoretical proposal in [51,52], a superconducting quantum interference device (SQUID) was used to impose a magnetically tunable boundary condition to the electromagnetic field in a coplanar waveguide, analogous to an effective mirror whose spatial position is controlled by the applied magnetic field. When the position of this (analog) mirror is made to oscillate in space via a suitable modulation of the magnetic field threaded through the SQUID, a sizable DCE emission into the waveguide was observed, spectrally centered at half the modulation frequency and displaying peculiar quantum optical properties expected in the DCE. Since no mechanically moving element was present, the experiment belongs to the class of analog models. However, its quantum evolution equations are identical to the one of the standard DCE effect. A related DCE experiment was published shortly after in [55]: in contrast to the analog mirror implemented in [54], here the optical length of the cavity was modulated by flux biasing the embedded SQUIDs so to slightly vary the effective refractive index.

Whereas the objective of this first generation of experiments was to detect the analog DCE emission and characterize its quantum statistical properties, a theoretical study of backreaction effects in all-optical analog models of DCE was reported in [56]. A strong and experimentally observable signal of backreaction was anticipated there, still the proposed device required a quite complex optical setup and the connection to the general physics of DCE remained nontrivial. It is therefore important to devise configurations that allow for a direct insight into the basic physics of backreaction.

The last part of this article indeed reports a theoretical study in this direction. A direct extension of the device proposed in [51,52] and experimentally realized in [54] is investigated: going beyond these works, the key idea is no longer to drive the SQUID with a classical, predetermined external field $B(t)$, but to magnetically couple it to an external LC resonator that plays the role of the harmonically moving mirror. Treating the LC resonator as an independent dynamical degree of freedom, we show that the equations describing the coupled dynamics of the LC and the waveguide are equivalent to the ones for a perfect, harmonically trapped mirror interacting with a quantum electromagnetic field via its radiation pressure [57]. Most remarkably, our quantitative estimates for the strength of the analog optomechanical coupling between the effective moving mirror and the cavity turn out to be promising in view of the observation of the backreaction effect with state-of-the-art technology.

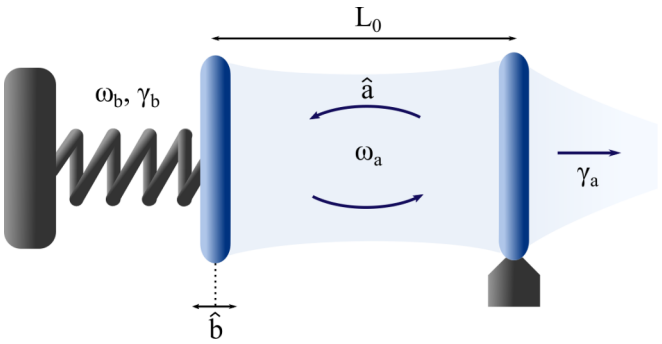

FIG. 1. Illustrative representation of a generic optomechanical system. One of the cavity mirrors is allowed to harmonically oscillate around the position of equilibrium and is optomechanically coupled to the cavity mode via the radiation pressure.

The article is organized as follows. We start by introducing in Sec. II the physical system at hand and by revising the fundamental concepts of the optomechanical interaction between the mechanical and electromagnetic degrees of freedom. In Sec. III A we then briefly review the mean-field theory of the system dynamics, which models the evolution of the system in the classical limit. In order to describe strictly quantum effects such as particle creation from DCE and the backreaction effects, a more sophisticated theory going beyond the mean-field approximation is developed in Sec. III B. The key results of our theoretical study of the backreaction effect are presented in Sec. IV. The observable consequences of the backreaction are first investigated in Sec. IV A for the case of an initially displaced mirror that performs free oscillations while interacting with the cavity mode. For relatively weak optomechanical coupling strength, the backreaction results in a reinforced damping of the mechanical oscillation. For coupling strengths stronger than the loss rate, the backreaction results instead in a periodic and reversible exchange of energy between the mirror and the field. In Sec. IV B we then study the related but different case where the mirror is mechanically driven by a monochromatic external force: for a weak optomechanical coupling, the backreaction effect is visible as a broadened line shape for the resonant mechanical response of the mirror. For stronger couplings, we anticipate a splitting of the resonant response into a pair of Rabi-split peaks as well as a number of other nonlinear features. A promising strategy to experimentally investigate this physics in an circuit-QED-based analog model is quantitatively discussed in Sec. V. Conclusions and future perspectives are finally given in Sec. VI.

II. THE SYSTEM

We begin our discussion from a study of the backreaction effect in its original formulation in terms of a friction force acting on the mechanically moving mirror. The system under consideration is sketched in Fig. 1: it consists of an optical cavity terminated on one side by a mechanically moving mirror of mass m_b, confined around its equilibrium position by a harmonic potential of characteristic angular frequency

ω_b. For the sake of simplicity, we restrict the dynamics of the field to a single relevant mode of the optical cavity and we indicate with ω_a the frequency of the cavity mode when the mirror is at its equilibrium position and the cavity has length L_0.

Defining by $\hat{a}$ ($\hat{a}^\dagger$) and $\hat{b}$ ($\hat{b}^\dagger$) the annihilation (creation) operators for the field and the mechanical oscillator, respectively, the Hamiltonian $\hat{H}_0$ for the noninteracting system takes the simple form

$$\hat{H}_0 = \hbar\omega_a \hat{a}^\dagger \hat{a} + \hbar\omega_b \hat{b}^\dagger \hat{b}. \tag{1}$$

The mirror and the field interact with each other via the radiation pressure, defined in terms of a pressure operator $\hat{P}$ which depends quadratically on the field [57],

$$\hat{P} = \frac{\hbar\omega_a}{2L_0}(\hat{a} + \hat{a}^\dagger)^2. \tag{2}$$

In terms of the displacement operator for the mirror around its equilibrium position $\hat{x} = x_{\mathrm{ZPF}}(\hat{b} + \hat{b}^\dagger)$, where $x_{\mathrm{ZPF}} = (\hbar/2m\omega_b)^{1/2}$ is the amplitude of the mechanical zero-point fluctuations, the optomechanical pressure interaction is described by the Hamiltonian [33]

$$\hat{H}_{\mathrm{int}} = -\hat{x}\hat{P} = -\hbar\omega_c(\hat{a} + \hat{a}^\dagger)^2(\hat{b} + \hat{b}^\dagger), \tag{3}$$

where the strength of the optomechanical coupling between the mechanical and electromagnetic degrees of freedom is quantified by the effective interaction frequency

$$\omega_c = \frac{\omega_a x_{\mathrm{ZPF}}}{2L_0} = \frac{\omega_a}{L_0}\left(\frac{\hbar}{8m_b\omega_b}\right)^{1/2}. \tag{4}$$

For the sake of simplicity, we assume from now on that the system in a regime where the optomechanical coupling is much weaker than the natural oscillation frequencies of both the cavity and the mechanical mirror, $\omega_c/\omega_{a/b} \ll 1$. Such an assumption does not represent a significant limitation for our purposes, but allows us to neglect extra effects such as the dressing of the mirror by virtual photons and the consequent modification of the ground state of the interacting system [58]. More specifically, under this condition the effects of antiresonant terms of the Hamiltonian in Eq. (3) like $\hat{a}^\dagger\hat{a}\hat{b}$, $\hat{a}^2 b$, and $(\hat{a}^\dagger)^2 b^\dagger$ can be neglected, as they are responsible for a minor correction to the energy levels of the system [59]. The optomechanical coupling is thus modeled by the resonant terms $\hat{a}^2\hat{b}^\dagger$, $(\hat{a}^\dagger)^2\hat{b}$ only, which describe the creation (annihilation) of mechanical excitations in the mirror and the simultaneous annihilation (creation) of a pair of photons. This is the physical mechanism responsible for the DCE, and thus for the exchange of energy between the mirror and the field and, in the final instance, for the appearance of friction in the mechanical motion of the mirror. A more general numerical approach that includes the ultrastrong coupling limit $\omega_c/\omega_{a/b} \gtrsim 1$ and the effects of the antiresonant terms was recently pursued in [37].

We consider that both the mirror and the cavity mode are coupled to external degrees of freedom. In particular, we assume that the mirror is mechanically driven by an external coherent force of amplitude $F(t)$, which can be modeled by means of additional time-dependent terms in the Hamiltonian

$$\hat{H}_{\mathrm{drive}} = -\hbar(\hat{b}F^*(t) + \hat{b}^\dagger F(t)). \tag{5}$$

Summing up all terms, the coherent dynamics of the system is modeled by the total Hamiltonian

$$\begin{aligned}\hat{H} &= \hat{H}_0 + \hat{H}_{\mathrm{int}} + \hat{H}_{\mathrm{drive}} \\ &= \hbar\omega_a\hat{a}^\dagger\hat{a} + \hbar\omega_b\hat{b}^\dagger\hat{b} + \hbar\omega_c(\hat{b}^\dagger\hat{a}^2 + \hat{b}(\hat{a}^\dagger)^2) \\ &\quad - \hbar(\hat{b}F^*(t) + \hat{b}^\dagger F(t)).\end{aligned} \tag{6}$$

On top of this, we take into account losses in the system by coupling the optical field to an external radiative and/or nonradiative baths and by including mechanical dissipation damping the mirror motion. Both these effects are included at the level of the master equation, so that the time evolution of the density matrix $\hat{\rho}$ of the interacting mirror-field system has the form

$$\frac{d\hat{\rho}}{dt} = \frac{1}{i\hbar}[\hat{H}, \hat{\rho}] + \mathcal{L}_{\hat{a}}[\hat{\rho}] + \mathcal{L}_{\hat{b}}[\hat{\rho}], \tag{7}$$

in terms of the Lindblad superoperators

$$\mathcal{L}_{\hat{o}} \equiv (\gamma_o/2)(2\hat{o}\hat{\rho}\hat{o}^\dagger - \hat{o}^\dagger\hat{o}\hat{\rho} - \hat{\rho}\hat{o}^\dagger\hat{o}) \tag{8}$$

describing cavity and mechanical losses with $\hat{o} = \hat{a}, \hat{b}$, respectively. Equation of motion for expectation value of generic observables $\hat{O}$ can finally be obtained from the master equation,

$$\begin{aligned}\frac{d\langle O\rangle}{dt} &= \frac{1}{i\hbar}\mathrm{Tr}_S\{[\hat{O}, \hat{H}]\hat{\rho}\} \\ &\quad + \sum_{\hat{o}=\hat{a},\hat{b}} \frac{\gamma_o}{2}(\mathrm{Tr}\{[\hat{o}^\dagger, \hat{O}]\hat{o}\,\hat{\rho}\} + \mathrm{Tr}\{\hat{o}^\dagger[\hat{O}, \hat{o}]\hat{\rho}\}).\end{aligned} \tag{9}$$

In the next sections we are going to develop a formalism to obtain explicit results for the quantum system dynamics, which is able to go beyond the mean-field approximation and take into account the quantum fluctuations of the field at the simplest level. Based on this, we will provide a quantitative estimate for the friction due to the emission of dynamical Casimir pairs, and we will compare the analytical results with the full numerical solution of the master equation in Eq. (7).

III. THEORETICAL MODELS

A. Mean-field theory of the parametric oscillator

The cubic nature of the Hamiltonian in Eq. (6) makes the solution of the interacting field-mirror problem far from trivial. Simplifying hypotheses are thus needed, in order to derive approximate solutions which are able to capture at least some of the most significant properties of the system. We begin our discussion from a semiclassical approximation, where one focuses on the average value of the field and mirror oscillation amplitudes and replaces the $\hat{a}$ and $\hat{b}$ operators with the corresponding classical variables $a \equiv \langle\hat{a}\rangle$ and $b \equiv \langle\hat{b}\rangle$. The equations of motion for such *mean fields* can be derived from the master equation.

Assuming that the drive is monochromatic $F(t) = F_0\, e^{-i\omega t}$ with given amplitude F_0 and frequency ω, we can usefully move to the frame rotating with the angular frequency ω of the drive. Within the rotating frame, the annihilation operators transform to $\hat{a} \to \hat{a}\, e^{-i\omega t/2}$ and $\hat{b} \to \hat{b}\, e^{-i\omega t}$, so that the

equation of motion for the expectation values get the autonomous form

$$\frac{da}{dt} = -\left(\frac{\gamma_a}{2} - i\Delta_a\right)a - 2i\omega_c a^* b, \tag{10}$$

$$\frac{db}{dt} = -\left(\frac{\gamma_b}{2} - i\Delta_b\right)b - i\omega_c a^2 + iF_0, \tag{11}$$

where we defined the detuning $\Delta_a \equiv \omega/2 - \omega_a$ and $\Delta_b \equiv \omega - \omega_b$. Given the dissipative form of Eqs. (10) and (11), a steady-state solution can be derived by setting the time derivatives to zero. These equations have the simplest form in the fully resonant case where the drive is resonant with the mirror frequency ($\omega = \omega_b$) and this latter is in resonance with twice the optical frequency ($\omega_b = 2\omega_a$).

In these conditions the system exhibits a sort of phase transition at the threshold value $F_0 = F_0^{\rm th} \equiv \gamma_a\gamma_b/8\omega_c$ of the drive amplitude, at which the solution

$$a_B = 0, \tag{12}$$

$$b_B = \frac{2i}{\gamma_b}F_0, \tag{13}$$

which is stable below the threshold $F_0 < F_0^{\rm th}$, becomes dynamically unstable. Above threshold, the system spontaneously break a Z_2 symmetry and has the choice to migrate towards two possible different branches, characterized by the same mirror amplitude but equal and opposite values of the field amplitude,

$$a_A^{\pm} = \pm\left(\frac{F_0 - F_0^{\rm th}}{\omega_c}\right)^{1/2}, \tag{14}$$

$$b_A = i\frac{\gamma_a}{4\omega_c}. \tag{15}$$

The parametric oscillator threshold at $F_0^{\rm th}$ thus separates two qualitatively different regimes of the system. *Below* the threshold, the classical component of the cavity field is zero, while the average amplitude of the mechanical oscillations increase linearly with the strength of the applied drive. As we shall see shortly, in this regime the quantum fluctuations of the field play a major role in determining the quantum state of the cavity field. Conversely, *above* the threshold, the expectation value of the field is finite and the mirror amplitude saturates to a finite value. In this case the system behaves to a good approximation classically, with the quantum fluctuations accounting only for small corrections to the mean-field dynamics. For later convenience we define $\gamma_0^2 \equiv \gamma_a\gamma_b/2$, so that $F_0^{\rm th} = \gamma_0^2/4\omega_c$.

While this classical model is typically able to reproduce the general trend of the steady-state field expectation values, it is not able to capture strictly quantum effect, such as the parametric amplification of vacuum fluctuations of the electromagnetic field via the dynamical Casimir effect and, in turn, the backreaction of the dynamical Casimir photons onto the mechanical degrees-of-freedom. This can be directly seen from the mean-field steady state below threshold found above, which contains no cavity excitation $a_B = 0$.

Generalization of the steady-state solutions (12) and (13) to general values of Δ_b further shows that the response function of the oscillator to the external drive has the form of a Lorentzian function with central frequency ω_b, and a linewidth equal to the damping rate γ_b of the bare mechanical oscillator

$$|b(\omega)|^2 = \frac{|F_0|^2}{\Delta_b^2 + (\gamma_b/2)^2}. \tag{16}$$

The absence of any Casimir emission and any backreaction effect shows that in order to understand the physics of these effects it is necessary to go beyond the mean-field approximation and include quantum fluctuations in the model. This will be the objective of the following sections.

B. Beyond mean field

In order to go beyond the mean-field theory, we first note that, because of the symmetry properties of the Hamiltonian in Eq. (6), the expectation value of any correlator containing an odd number of cavity field annihilation and creator operators $\hat{a}, \hat{a}^\dagger$ does not change in time under the Hamiltonian evolution and remains strictly zero in the steady state. The fundamental dynamical quantities for the field are thus given by the quadratic operators $\hat{q} \equiv \hat{a}^2$ and $\hat{n}_a \equiv \hat{a}^\dagger\hat{a}$.

On this basis, a simple description of the quantum dynamics of the system can be formulated in terms of the time evolution of the expectation values of the amplitudes $b \equiv \langle\hat{b}\rangle$ and $q \equiv \langle\hat{q}\rangle$ for the mirror and the cavity field, respectively, and of the number of photons in the cavity $n_a \equiv \langle\hat{n}_a\rangle$. Working again in the frame rotating at the drive frequency ω, we can describe the system by the set of three equations:

$$\frac{db}{dt} = -\left(\frac{\gamma_b}{2} - i\Delta_b\right)b - i\omega_c q + iF_0, \tag{17}$$

$$\frac{dn_a}{dt} = -\gamma_a n_a - 2i\omega_c\langle q^\dagger b\rangle + 2i\omega_c\langle qb^\dagger\rangle, \tag{18}$$

$$\frac{dq}{dt} = -(\gamma_a - i\Delta_q)q - 4i\omega_c\langle n_a b\rangle - 2i\omega_c b, \tag{19}$$

where we defined the detuning $\Delta_q \equiv \omega - 2\omega_a$. Equations (17)–(19) reveal how the presence of cubic terms in the Hamiltonian Eq. (6) leads to an infinite hierarchy of correlators that need to be suitably truncated in order to obtain a solution to the problem. This effectively means neglecting the correlation of higher order between the mirror and the field, and attention must be paid to the conditions under which this approximation is justified. To this aim we identify three different regimes.

(i) In the limit of a weak drive $F_0 \ll F_0^{\rm th}$, the correlators involving products of two $\hat{b}$, $\hat{q}$, and $\hat{n}_a$ operators can be safely neglected as they represent higher order terms in the infinitesimal quantities q, b, and n_a. From now on, this regime will be called *linear regime*, since in this case Eqs. (17)–(19) reduce to a set of three linear equations. In spite of its simplicity, this linear model is able to account for the quantum fluctuations responsible for the DCE emission and, then, for the backreaction effect.

(ii) In the opposite limit of a strong drive $F_0 \gg F_0^{\rm th}$, the system is in the parametric oscillator limit. As mentioned in the previous section, in this regime the system behaves in an

approximately classical way: the nonfactorizable component (that is the *cumulant* in the language of statistics) in the correlations between the field and the mirror can be neglected and the correlations can be factorized as $\langle a^2 b^\dagger\rangle \simeq q b^*$ and $\langle a^\dagger a b\rangle \simeq n_a b$ (we indicated by asterisk "*" the complex conjugate operation). The equations of motion (17)–(19) then reduce to the closed *nonlinear* system

$$\frac{db}{dt} = -\left(\frac{\gamma_b}{2} - i\Delta_b\right)b - i\omega_c q + iF_0, \tag{20}$$

$$\frac{dn_a}{dt} = -\gamma_a n_a - 2i\omega_c q^* b + 2i\omega_c q b^*, \tag{21}$$

$$\frac{dq}{dt} = -(\gamma_a - i\Delta_q)q - 4i\omega_c n_a b - 2i\omega_c b. \tag{22}$$

(iii) In the region of parameters between these two limits, that is for $F_0 \sim F_0^{\rm th}$, quantum fluctuations play a crucial and complex role and the nontrivial higher order correlations between the field and the mirror need to be fully taken into account to properly describe the properties of the system.

For the purpose of this article, we note that the best conditions for the investigation of the backreaction effects from the DCE photons are met in the linear regime of weak drive and weak excitation. In this case, all the key features of the DCE mechanism are kept in play, with the advantage of being able to neglect all the complex nonlinear effects arising from the radiation pressure coupling of the field with the mechanical oscillator. As we will see in the next sections, this simplifies very much the analysis, and closed expressions for the quantities of interest can be obtained by analytical means.

IV. VACUUM-INDUCED FRICTION

In the previous sections we have introduced the physical model under consideration and the theoretical tools that can be used to study its nonequilibrium dynamics. In this section we investigate the central subject of the article, namely the observable signatures of the backreaction effect of the dynamical Casimir emission onto the mechanically moving mirror. In the next two subsections, this backreaction effect will be studied in the two most relevant cases of the ring-down oscillations of a freely oscillating mirror and of a mechanically driven mirror subject to a monochromatic force.

A. Free evolution

We start our study of the backreaction effect from the case of the free evolution of the mirror: the physical idea is that the cavity is prepared in its vacuum state, while the mirror is prepared in a coherent state with a given amplitude. Starting from this state, the system is then let to evolve in the absence of any external drive $F_0 = 0$. The dissipative nature of the evolution will eventually bring it back to the ground state with all fields being in their vacuum state, but the intermediate dynamics will carry interesting signatures of the dynamical Casimir and of the backreaction effects.

To investigate this physics, we go back to the full set in Eqs. (17)–(19). In absence of the external drive, that is for $F_0 = 0$, there is no advantage in moving to the rotating frame for the operators. We start from the simplest and most relevant regime of a small initial perturbation from the ground state, in which case the equations can be linearized into the form

$$\frac{db}{dt} = -i\omega_b b - \frac{\gamma_b}{2}b - i\omega_c q, \tag{23}$$

$$\frac{dq}{dt} = -(\gamma_a - 2i\omega_a)q - 2i\omega_c b, \tag{24}$$

which describe a damped oscillating evolution for both the mirror and the field amplitude starting from the initial conditions $b(0) = b_0$ and $q(0) = 0$. These equations of motion can be analytically solved and, in the resonant case $\omega_b = 2\omega_a$, provide the solutions

$$b(t) = e^{-i\omega_b t - \gamma_1 t/2}\frac{b_0}{2\omega_d}\left[\left(\gamma_a - \frac{\gamma_b}{2}\right)\sin(\omega_d t) + 2\omega_d\cos(\omega_d t)\right], \tag{25}$$

$$q(t) = e^{-2i\omega_a t - \gamma_1 t/2}\frac{b_0}{4\omega_d\omega_c}\left[\left(\gamma_a - \frac{\gamma_b}{2}\right)^2 - 4\omega_d^2\right]\sin(\omega_d t), \tag{26}$$

which show a complex temporal envelope modulating the free oscillations of $b(t)$ and $q(t)$ at $\omega_b = 2\omega_a$. A similar expression can be obtained also for the average number of photons n_a, but we do not report it here because it is quite involved and not that instructive. For the sake of compactness, we have used the shorthands $\gamma_1 = \gamma_a + \gamma_b/2$ for the averaged dissipation rate and

$$\omega_d = \sqrt{2\omega_c^2 - (\gamma_a - \gamma_b/2)^2/4} \tag{27}$$

for the effective energy exchange frequency. Given the even symmetry of Eq. (25) with respect to ω_d, either of the two roots can be chosen. As a key result of this work, and in agreement with the conclusions of the recent work [37], we easily see that two regimes can be identified, depending on the relative values of the interaction frequency ω_c and the dissipation rates γ_a and γ_b, i.e., the real vs imaginary nature of ω_d.

In the *underdamped* $\omega_c > (\gamma_a - \gamma_b/2)/(2\sqrt{2})$ regime, the exchange frequency ω_d is real and energy is periodically exchanged between the mirror and the optical mode of the cavity, before being eventually damped with an exponential law on a longer timescale. In the opposite *overdamped* regime, damping is so large that ω_d is purely imaginary and the amplitude of the mirror oscillations is monotonically damped out. Of course the resulting damping rate gets contributions from the bare decay rate γ_b as well as from the backreaction effect. In the weak optomechanical regime $\omega_c \ll \gamma_{a,b}$ and assuming $\gamma_a \gg \gamma_b$, the reinforced damping reads

$$\gamma_b^{\rm eff} \simeq \gamma_b + \frac{4\omega_c^2}{\gamma_a}. \tag{28}$$

Since the dynamical Casimir emission is suppressed for substantial values of the mirror-cavity detuning $|\omega_b - 2\omega_a| \gg \gamma_{a,b}$, the backreaction contribution can be isolated by comparing the values of the damping rate that are observed in the two cases when the cavity is tuned respectively on or far-off resonance from the mirror.

This linearized approach holds for weak initial amplitudes $b_0^2 \ll \gamma_a^2/\omega_c^2$, so that the nonlinear terms in the motion

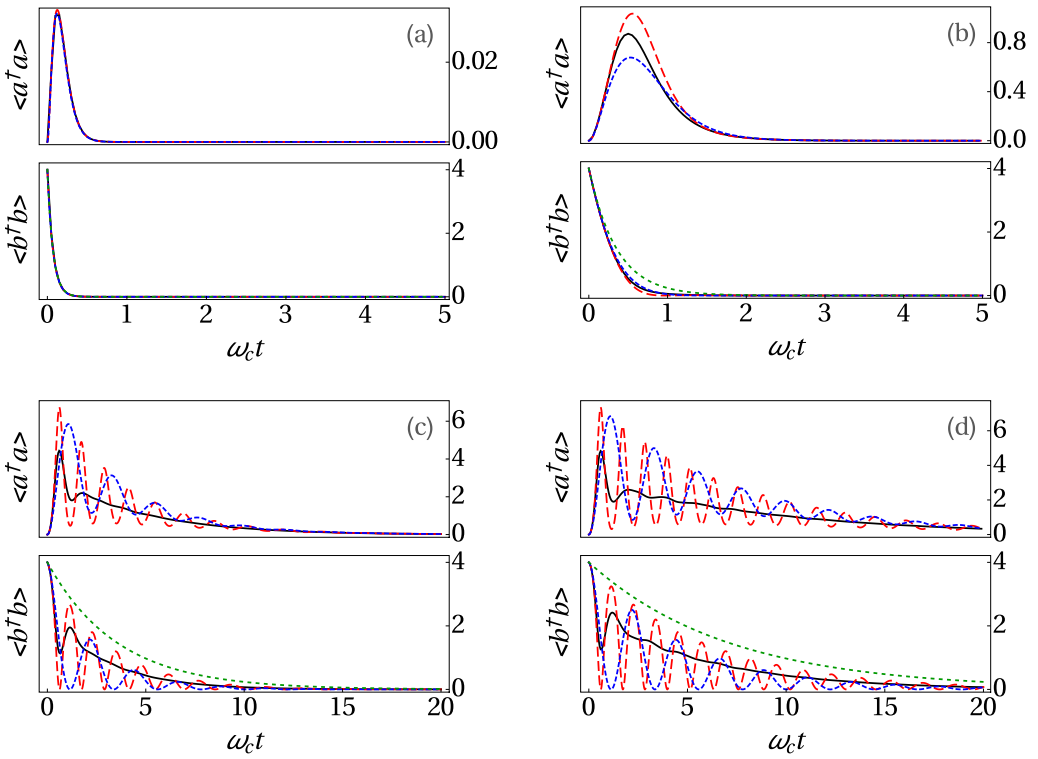

FIG. 2. Free evolution of the interacting cavity field-mirror system. At the initial time $t = 0$, the cavity field is in its vacuum state, while the mechanical oscillator is in a coherent state of amplitude $b_0 = 2$. Solutions are given in terms of the number of photons in the cavity $\langle \hat{a}^\dagger \hat{a} \rangle$ and of mechanical oscillator quanta $\langle \hat{b}^\dagger \hat{b} \rangle$. The different panels (a)–(d) are for growing values of the ratio $\omega_c/\gamma_0 = 0.1, 0.5, 5, 10$. In each panel, the solution (L) of the linearized equations is plotted as a blue fine dashed line, the solution (NL) of the nonlinear mean-field equations is shown as a dashed red line, and the full numerical solution (ME) of the master equation Eq. (7) is shown as a continuous (black) line. In the panels for $\langle \hat{b}^\dagger \hat{b} \rangle$, the dotted green lines [not distinguishable in (a)] show the evolution of the mirror in the absence of optomechanical coupling to the cavity field, that is for $\omega_c = 0$.

equations are negligible. In a more general case, the full quantum nonlinear equations (17)–(19) should be considered. For small values of $\omega_c/\gamma_{a,b}$, one can expect that nonlinear mean-field equations (20)–(22) should provide a reasonable approximate description.

These analytical expectations are validated in Fig. 2 which shows the free evolution of the system starting from $b_0 = 2$ and the cavity field in its vacuum state. The Figs. 2(a)–2(d) refer to growing values of coupling strength, $\omega_c/\gamma_0 = 0.1,\ 0.5,\ 5,\ 10$. In each panel, the different curves show the full numerical solution of the master equation (black solid line), the solution of the linearized equations (blue dotted line), and the solution of the nonlinear mean-field equations (red dashed line). The dotted green lines in the panels for $\langle \hat{b}^\dagger \hat{b} \rangle$ show the bare damping of the mechanical oscillator at γ_b. For simplicity we have assumed equal dissipation rates for both the cavity and the mechanical oscillator $\gamma_a = \gamma_b = \gamma$, so that $\gamma_0 = \gamma/\sqrt{2}$ and $\gamma_1 = 3\gamma/2$. With this choice, one has $\omega_d = (2\omega_c^2 - \gamma^2/16)^{1/2}$.

In Fig. 2(a) we illustrate the overdamped regime of weak optomechanical coupling: while the mechanical oscillator performs a monotonic decay towards its ground state, the cavity field is initially excited by the dynamical Casimir effect, then the photons are lost by dissipation. Consequences of backreaction can be found in the decay rate of the mirror oscillation, which is reinforced compared to its bare value γ_b (green dotted line). The quantitative importance of this effect grows with ω_c: while it is almost invisible on the scale of Fig. 2(a), it shows up clearly in Fig. 2(b). In both these panels, the agreement of the different approximations to the full numerical solution is very good and the discrepancy gets smaller as ω_c/γ_0 is decreased.

In Figs. 2(c) and 2(d) we illustrate the underdamped regime where a continuous and periodic transfer of energy occurs between the mirror and the field and vice versa. The timescale on which such a conversion takes place can be estimated from the analytical theory to be on the order of $1/\omega_d$. Because of the losses, the system then decays towards the vacuum state on a timescale set by the characteristic time $1/\gamma_1$. Given the relatively large initial value of b chosen here, the linearized approach provides inaccurate results. The nonlinear mean-field equations are however able to reasonably capture the oscillation frequency. Quantum fluctuations and correlations are then responsible for the quick damping of the oscillations shown in the full numerics.

B. Driven-dissipative steady state under a monochromatic drive

After having discussed the free evolution of the system under the combined effect of the losses and the dynamical Casimir emission, we now turn to the driven-dissipative dynamics when the system is continuously driven by a

monochromatic drive acting on the mirror. As we have done in the previous section, the full numerical results will be compared to the solution of the nonlinear equations (20)–(22): as compared to the pure mean-field theory based on one-operator expectation values of Sec. III A, these equations explicitly include the relevant two-operator quantities that enter into the DCE, in particular $q = \langle \hat{a}^2 \rangle$.

1. Linear regime

We start from the case where the strength of the external drive is small enough that the system is slightly perturbed from the vacuum. In this regime, an analytical solution for the response of the mirror can be obtained by linearizing the equations of motion, which gives

$$b(\omega) = \mathcal{R}(\omega) F_0, \tag{29}$$

where $\mathcal{R}(\omega)$ is the response function of the oscillator

$$\mathcal{R}(\omega) = -\frac{\Delta_q + i\gamma_a}{\Delta_b \Delta_q + i\left(\gamma_a \Delta_b + \frac{\gamma_b}{2}\Delta_q\right) - \left(2\omega_c^2 + \gamma_0^2\right)}. \tag{30}$$

This formula is one of the key results of our work. In the completely resonant case $\omega_b = 2\omega_a$, it simplifies as

$$\mathcal{R}(\omega) = -\frac{\Delta + i\gamma_a}{\Delta^2 + i\gamma_1 \Delta - \left(2\omega_c^2 + \gamma_0^2\right)}, \tag{31}$$

where $\Delta = \omega - \omega_b = \omega - 2\omega_a$. As expected, in the limit $\omega_c \to 0$ of a vanishing optomechanical interaction, the response function reduces to the response (16) of the bare oscillator.

For small $\omega_c \ll \gamma_{a,b}$, and assuming for simplicity $\gamma_a \gg \gamma_b$, the response (31) takes the Lorentzian form

$$\mathcal{R}(\omega) = \frac{1}{\Delta + i\gamma_b^{\text{eff}}/2}, \tag{32}$$

with the effective damping rate for the mirror given in Eq. (28). This last formula clearly shows the backreaction effect of the dynamical Casimir emission as a reinforced broadening of the mirror response: while the first term in Eq. (28) is the bare damping of the mechanical oscillator, the second term accounts for the damping due to the creation of photon pairs out of the vacuum. Since the dynamical Casimir effect is dramatically suppressed far away from resonance $|\omega_b - 2\omega_a| \gg \gamma_{0,1}$, the backreaction contribution can be extracted just by looking at the dependence of the linewidth on the cavity-mirror detuning $\omega_b - 2\omega_a = \Delta_q - \Delta_b$. Of course, isolating the backreaction contribution to the mechanical dissipation requires that the intrinsic dissipations $\gamma_{a,b}$ are not far larger than the optomechanical coupling ω_c.

For arbitrary values of ω_c, the squared amplitude of the mirror oscillations follows directly from Eq. (31),

$$|b(\omega)|^2 = \frac{\Delta^2 + \gamma_a^2}{\left[\Delta^2 - \left(2\omega_c^2 + \gamma_0^2\right)\right]^2 + \gamma_1^2 \Delta^2} |F_0|^2. \tag{33}$$

For strong values of the coupling $\omega_c \gg \gamma_{a,b}$, the periodic energy exchange between mechanical and optical modes predicted in the previous section manifests itself in a complex response spectrum showing a pair of Lorentzian peaks of width γ_1 separated by a splitting approximately given by $2\sqrt{2}\omega_c$,

$$|b(\omega)|^2 = \frac{2\omega_c^2}{\left(\Delta^2 - 2\omega_c^2\right)^2 + 2\omega_c^2 \gamma_1^2} |F_0|^2. \tag{34}$$

Quantitatively, for typical parameters of high-frequency optomechanical systems taken from [60], the optomechanical coupling results on the order of $\omega_c \approx 1$ Hz. As we have seen in this section, weak optomechanical couplings require correspondingly small dissipation rates $\gamma \lesssim \omega_c$ for the backreaction effect to be observable, which is anticipated to pose serious difficulties to experimental verification of our predictions.

2. Nonlinear mean-field regime

For higher strength of the drive, calculation of the response of the system need to include the nonlinear character of the system, encoded in Eqs. (20)–(22). Since we are interested in the stationary state of the system, we pose the time derivatives to zero here. To analytically tackle the nonlinear equation, we combine the first and the second ones to find the steady state for the mirror oscillation amplitude and for the field fluctuations as a function of the average number of photons in the cavity n_a,

$$b = \frac{(\Delta + i\gamma_a) F_0}{\left[2\omega_c^2 (1 + 2n_a) - \left(\Delta^2 - \gamma_0^2\right)\right] - i\Delta\gamma_1}, \tag{35}$$

$$q = \frac{2\omega_c (1 + 2n_a) F_0}{\left[2\omega_c^2 (1 + 2n_a) - \left(\Delta^2 - \gamma_0^2\right)\right] - i\Delta\gamma_1}. \tag{36}$$

Here we posed $\omega_b = 2\omega_a$ (that is $\Delta_a = \Delta_b = \Delta$). From the third equation we then find a condition for $x \equiv (1 + 2n_a)$ in the form of a third order polynomial equation,

$$\omega_c^4 x^3 - \omega_c^2 \left[\omega_c^2 + \left(\Delta^2 - \gamma_0^2\right)\right] x^2 + \left[\frac{\left(\Delta^2 - \gamma_0^2\right)^2}{4} + \omega_c^2 \left(\Delta^2 - \gamma_0^2\right) + \frac{\Delta^2}{4}\gamma_1^2 - 4F_0^4\right] x - \frac{1}{4}\left(\left(\Delta^2 - \gamma_0^2\right)^2 + \Delta^2 \gamma^2\right) = 0, \tag{37}$$

which can be easily solved by numerical means. The solution then provides the amplitude of the mirror and field oscillations through Eqs. (35) and (36).

Because of the nonlinear nature of the problem, multiple (up to three) solutions could exist for these equations, depending on the values of the strength and frequency of the drive. Such *multistability* effects are well known in optics and a simplest example in our context is illustrated in Fig. 3: depending on the drive frequency, one or two stable solutions can be found, as well as a dynamically unstable one. The splitting of the two tilted peaks is due to a nonlinear Rabi coupling between the mechanical and optical degrees of

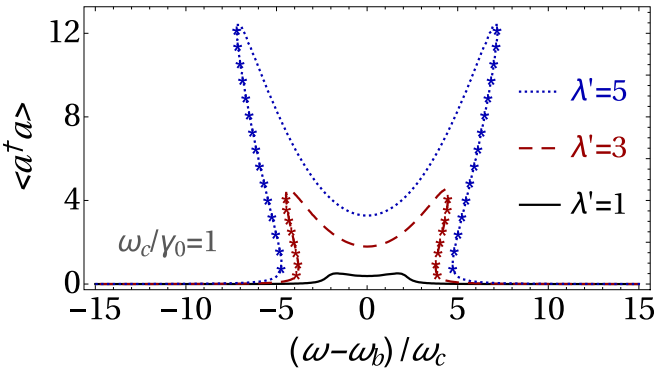

FIG. 3. Stationary state in the presence of a monochromatic mechanical drive acting on the mirror, in terms of the number of photons in the cavity as a function of the drive frequency ω. All curves are for the resonant case $\omega_b = 2\omega_a$, while different values $\lambda' = F_0/(F_0^{\rm th})' = 1,\ 3,\ 5$ for the drive amplitude are used. The presence of multiple solutions for the same drive frequency and amplitude indicate multistable behaviors, the dynamically unstable branches being highlighted by symbols.

freedom [61], and, for $n_a \gg 1$, can be estimated from (37) to be approximately $2\omega_c\, n_a^{1/2}$.

a. Modified parametric oscillator. This general theory can be successfully used to study the dynamical Casimir emission and the backreaction effect in the nonlinear regime. For simplicity we restrict ourselves to the fully resonant case $\omega = \omega_b = 2\omega_a$ and we give special attention to the field fluctuations, taken into account in our theory at the level of the averages of the $\hat{q}$ operator (we remind that $\hat{q} \equiv \hat{a}^2$). Setting $\Delta = 0$, Eqs. (35) and (36) simplify to

$$b = \frac{i\gamma_a\omega_c F_0}{2\omega_c^2 x + \gamma_0^2}, \tag{38}$$

$$q = \frac{2\omega_c^2 F_0}{2\omega_c^2 x + \gamma_0^2}, \tag{39}$$

while (37) reduces to

$$\omega_c^4 x^3 - \omega_c^2(\omega_c^2 - \gamma_0^2)x^2\left(\frac{\gamma_0^4}{4} - \omega_c^2\gamma_0^2 - 4\omega_c^4 F_0^2\right)x - \frac{\gamma_0^4}{4} = 0. \tag{40}$$

In the $F_0 \to 0$ limit, this set of equation admits the explicit solutions

$$b = \frac{i\omega_c\gamma_a F_0}{2\omega_c^2 + \gamma_0^2}, \quad q = \frac{2\omega_c^2 F_0}{2\omega_c^2 + \gamma_0^2}, \quad n_a = \frac{8\omega_c^4 F_0^2}{\left(2\omega_c^2 + \gamma_0^2\right)^2}, \tag{41}$$

which fully recover the result of the linearized equations (20)–(22). This is immediately seen, for example, by comparing the expression for b in Eq. (41) with the one in (29) and (31) for $\Delta = 0$.

In the opposite limit $F_0 \to \infty$, the nonlinear mean-field equations predict for the stationary state of the system

$$b = \frac{i\gamma_a}{4\omega_c}, \quad q = F_0, \quad n_a = F_0, \tag{42}$$

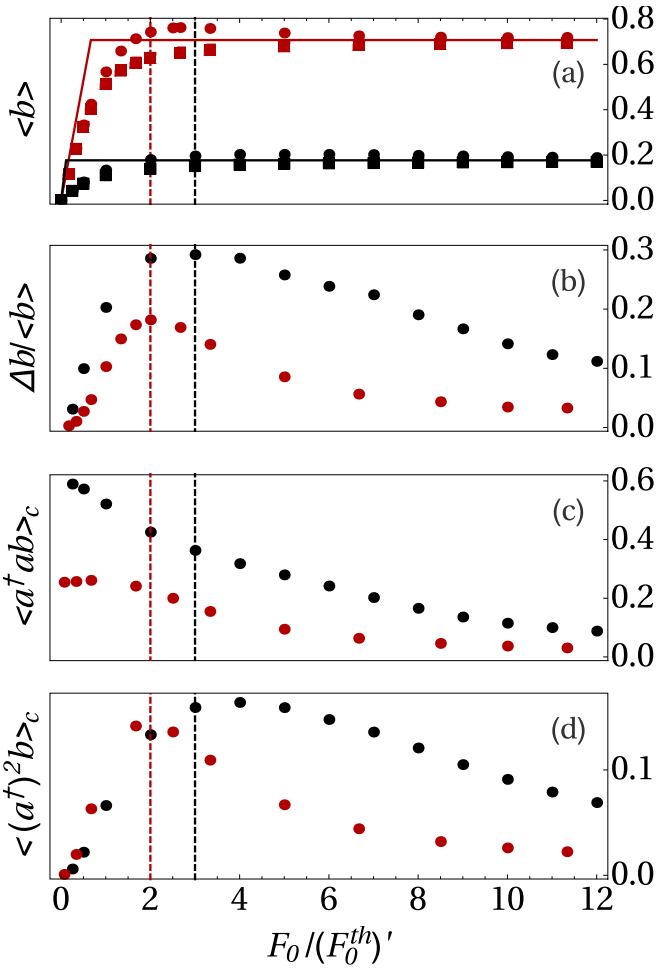

FIG. 4. Stationary state of the driven-dissipative evolution in the presence of a monochromatic drive acting on the mirror in a fully resonant condition $\omega = \omega_b = 2\omega_a$. (a) The amplitude of the mirror oscillations as a function of the drive amplitude. The solid line is the mean-field solution of (10) and (11), squares show the analytical nonlinear expression (40), and the circles indicate the full numerical prediction of the master equation. Different colors refer to different values of the optomechanical coupling $\omega_c/\gamma_0 = 0.5$ (red) and 2 (black). (b) The relative deviation between the analytical nonlinear solutions and the full numerical solution. (c) and (d) The numerical solutions for the normalized correlations between the field and the mirror, as defined in Eq. (44). Vertical dashed lines indicate the points of maximum deviation $\Delta b/\langle b\rangle$.

the equal expressions for q and n_a suggest that in this regime the cavity field is in a coherent state and its amplitude recovers the mean-field prediction (15).

The different dependence on the strength F_0 of the drive appearing in Eqs. (41) and (42) is a hint of the parametric oscillator transition. In order to estimate the amplitude of the drive at which the crossover between the below- and above-threshold regimes takes place, we equate the amplitude of the mechanical oscillations as predicted in Eqs. (41) and (42), obtaining the threshold value $(F_0^{\rm th})' = (1/2)(\omega_c + \gamma_0^2/2\omega_c)$. In the limit $\omega_c \to 0$, this expression reduces to the critical value $F_0^{\rm th}$ predicted by the mean-field theory. Such a transition is illustrated in Fig. 4(a), where the solution for b as a function

of F_0, for the values $\gamma_a/\sqrt{2} = \gamma_b/\sqrt{2} = \gamma/\sqrt{2} = 0.5,\ 2$ (that is for $\gamma_0 = 0.5,\ 2$, respectively), is shown. A close analysis of the figure reveals the existence of three distinct regimes depending on the value of the ratio $\lambda' \equiv F_0/(F_0^{\rm th})'$ of the drive strength. In contrast to the pure mean-field theory discussed in Sec. III A, the transition between the different regimes is not sharp but is smoothened out by quantum fluctuations.

The three regimes correspond to (i) *below* ($\lambda' \ll 1$), (ii) *above* ($\lambda' \gg 1$), and (iii) *around* ($\lambda' \simeq 1$) threshold. The solutions in Eq. (41) refer to the first of these regions [regime (i)]. The most interesting feature is that the quantum fluctuations due to the mirror-field interaction decrease the slope of b as a function of F_0 with respect to the mean-field prediction in Eq. (13) and this deviation grows with ω_c. All these elements confirm the origin of this feature in the DCE emission of photons that increases the effective damping of the mirror via the backreaction effect. Note also that, in this regime, the theoretical solution agrees very well with the (fully quantum) numerical one. This happens because, despite that the quantum fluctuations are not negligible in this limit and the factorization of the correlations is not justified, the system is only weakly displaced from its vacuum state, and the correlations account for higher order terms in the infinitesimal displacement of the system above its vacuum state.

Above the parametric oscillator transition [regime (iii)], the coherent oscillations of the mirror generated by the driving force are so large they induce a self-supported coherent oscillation in the cavity field as well. In the DCE context, such oscillations were observed in [62] and must, of course, be distinguished from the quantum-fluctuation-induced excitation that is observed in the cavity in regime (i) below the transition [54]. Also in regime (iii), the mean-field solution agrees well with both the theoretical and the numerical solutions: the system behaves in fact classically and quantum effects have a negligible impact on the dynamics.

In region (ii) in between these two limits, that is for values of the order $F_0 \sim (F_0^{\rm th})'$, the quantum fluctuations have non-negligible effects on the properties of the system, whose dynamics significantly deviates from the prediction of the theoretical model developed in the previous sections. These considerations are supported from the numerical results in Figs. 4(c) and 4(d), where the normalized correlations

$$\langle \hat{n}_a \hat{b} \rangle_c \equiv \frac{\langle \hat{n}_a \hat{b} \rangle}{n_a b} - 1, \tag{43}$$

$$\langle (\hat{a}^\dagger)^2 \hat{b} \rangle_c \equiv \frac{\langle (\hat{a}^\dagger)^2 \hat{b} \rangle}{q^* b} - 1 \tag{44}$$

are plotted as a function of the drive strength (we remind that by $q*$ we mean the complex conjugate of q, that is the expectation value $\langle \hat{q}^\dagger \rangle$). From the same figures, we also confirm the expectation that the stronger the optomechanical coupling is compared to the loss rates ω_c/γ_0, the stronger the effect of the quantum correlations and thus the larger are the deviations of the analytical results from the fully quantum numerical solution [Fig. 4(b)].

b. Spectral response. After having characterized the general features of the parametric transition in the fully resonant case, we now discuss the response of the mirror as a function of the drive frequency. In the linear regime of a weak drive, we obtained in Eqs. (33) that the linewidth of the response function gets an additional contribution from the backreaction effect of the DCE emission. The same conclusions can be drawn from the analysis of the more general nonlinear set of Eqs. (20)–(22), despite in this case an explicit solution for the response function cannot be obtained.

In Fig. 5 these predictions are contrasted with the corresponding numerical results. In Figs. 5(a)–5(c) we consider the case of a relatively weak $\omega_c/\gamma_0 = 0.5$ and different values of the drive strength $F_0/(F_0^{\rm th})' = 0.5,\ 2,\ 5$. We observe a good matching between the nonlinear analytical result and the numerical solution in the first and last cases, corresponding, respectively, to situations well below and well above the parametric oscillator transition. As expected, in the first case the linearized solution in Eq. (33) also provides a good approximation to the response function. A sizable deviation between the analytical and numerical results for the response function is instead observed in the intermediate case $F_0/(F_0^{\rm th})' = 2$, which is the value of the drive strength for which the discrepancy between the analytical and numerical solutions for $\Delta = 0$ was the largest in Fig. 4.

The response for a larger value $\omega_c/\gamma_0 = 2$ of the optomechanical coupling is shown in Fig. 5(d). The drive amplitude $F_0/(F_0^{\rm th})' = 3$ is again chosen to maximize the deviation between the analytical and numerical solutions for $\Delta = 0$ shown in Fig. 4. As expected, by comparing Figs. 5(b) and 5(d) we notice a better agreement between the two solutions in the case of a weaker optomechanical coupling.

V. CIRCUIT ANALOG

In the previous sections of this article, observable signatures of the backreaction effect have been identified in the relaxation dynamics of the system as well as in its response to an external drive. All these signatures will be of experimental interest as soon as a suitable optomechanical device is realized, in which the mechanical frequency is on resonance with the optical one $\omega_b \approx 2\omega_a$ to give a sizable dynamical Casimir emission and the optomechanical coupling is large enough to make the backreaction effect visible over other dissipation channels. As we have mentioned in the Introduction, this objective is however still facing great experimental difficulties, in particular for what concerns the mechanical frequency. In the first observation of dynamical Casimir emission [54], this difficulty was circumvented by making use of an analog model based on a superconductor-based waveguide. As theoretically proposed in [51,52], the role of the mirror is played here by a SQUID device and its mechanical motion in space is simulated by tuning the reflection phase of the SQUID via an externally imposed static magnetic field.

In this section we build atop all these works to propose and theoretically characterize a configuration where the mirror motion is not externally predetermined, but constitutes an independent degree of freedom of the system, dynamically coupled to the cavity field via the optomechanical Hamiltonian (3). The basic idea is to replace the externally imposed magnetic field with one generated by another, independent LC circuit concatenated to the SQUID. A possible implementation of this idea is sketched in Fig. 6. In contrast to the open-waveguide experiment [54], the opposite end of

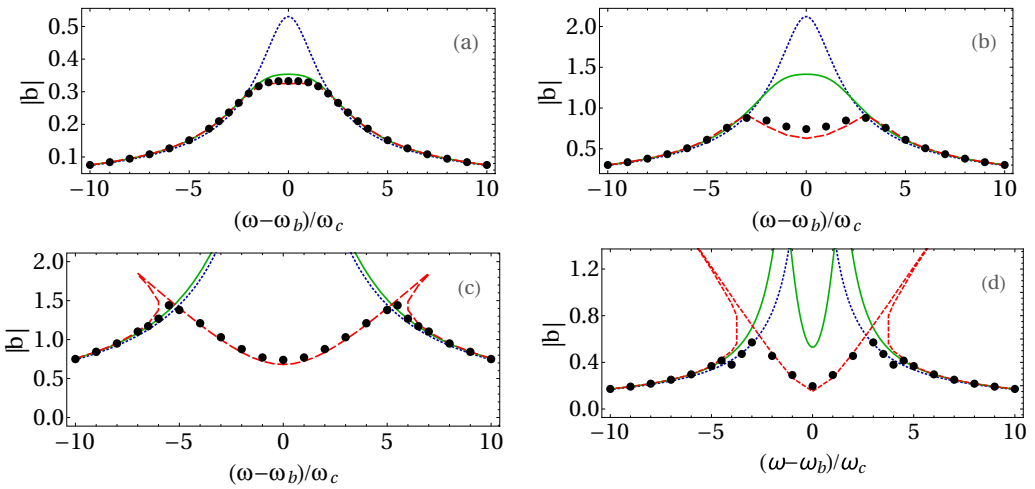

FIG. 5. Steady-state amplitude of the mirror oscillation as a function of the frequency ω of the monochromatic drive. We consider the mechanical oscillator resonant with the cavity field: $\omega_b = 2\omega_a$, and use different values for the optomechanical coupling and of the drive amplitude. (a)–(c) $\omega_c/\gamma_0 = 0.5$ and $F_0/(F_0^{\rm th})' = 0.5$ (a), $F_0/(F_0^{\rm th})' = 2$ (b), and $F_0/(F_0^{\rm th})' = 5$ (c). (d) $\omega_c/\gamma_0 = 2$ and $F_0/(F_0^{\rm th})' = 3$. The black symbols indicate the numerical solution of the master equation (7). The prediction of the linearized theory is shown as a solid green line. The prediction of the nonlinear mean-field model is shown as a dashed red line. The response of the bare mirror for a vanishing optomechanical coupling is shown as a dotted blue line.

the CPW terminates here on a highly reflecting capacitive gap, so to obtain discrete high-Q cavity modes as experimentally realized in [62]. Using experimental parameters from these works, a quantitative estimate for the effective optomechanical coupling which can be realistically obtained in state-of-the-art devices is obtained. Most remarkably, this value appears very promising in view of an experimental observation of the backreaction effect.

The starting point is the relation between the effective position $x_{\rm eff}$ of the analog mirror (measured from the physical position of the SQUID) and the magnetic flux ϕ threaded through the SQUID. Such a formula was derived in full detail in [52],

$$x_{\rm eff} = \left(\frac{\Phi_0}{2\pi}\right)^2 \frac{1}{\ell_{\rm wg} E_J(\phi)}, \tag{45}$$

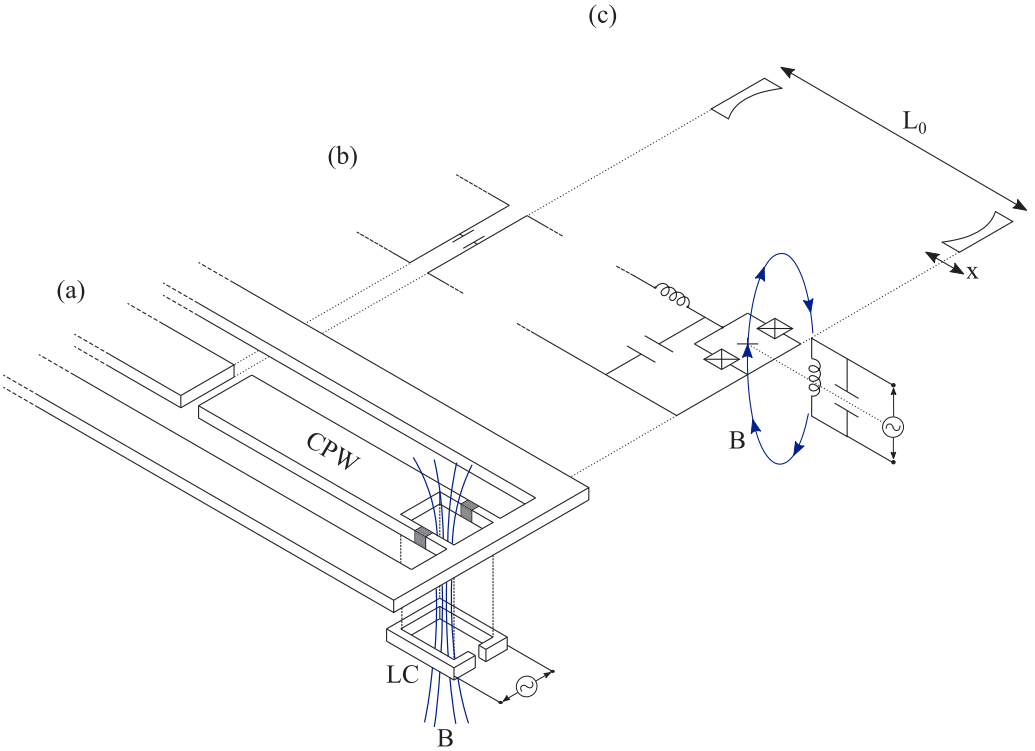

FIG. 6. (a) Pictorial representation of the LC resonator magnetically coupled to the coplanar waveguide. (b) Sketch of the equivalent circuit. (c) Effective cavity with moving mirror in correspondence of the SQUID.

where $\ell_{\rm wg}$ is the impedance per unit length of the waveguide, and Φ_0 is the quantum of magnetic flux. Here $E_J(\phi)$ is the (flux-dependent) Josephson energy of the SQUID, written as

$$E_J(\phi) = 2E_J^o\,|\cos(\pi\phi/\Phi_0)| \tag{46}$$

in terms of the single junction Josephson energy E_J^o. Provided the modulation frequency is much smaller than the plasma frequency of the SQUID $\omega_s = 2\pi\sqrt{2E_J^o/\Phi_0^2 C_J^o}$ (where C_J^o is the capacitance of each Josephson junction forming the SQUID), a small time-dependent flux $\delta\phi$ then results in a time-dependent variation of the effective cavity length

$$\delta x_{\rm eff} = -x_{\rm eff}\frac{\delta E_J(\phi)}{E_J(\phi)} = x_{\rm eff}\frac{\sin(\pi\phi/\Phi_0)}{\cos(\pi\phi/\Phi_0)}\frac{\pi\,\delta\phi}{\Phi_0}. \tag{47}$$

Assuming that the self-inductance of the SQUID is much smaller than the kinetic one, $L_{\rm SQUID} \ll [\Phi_0/(2\pi)]^2/E_J^o$, the former can be neglected. The magnetic flux threaded by the LC circuit through the SQUID can be written as $\delta\phi = MI_{\rm LC}$ in terms of the current $I_{\rm LC}$ flowing through the LC and the mutual inductance M, this latter being of course bounded from above by the self-inductance of the circuit $M/L_{\rm LC} < 1$.

Using the expression for the average magnetic energy stored in the ground state of the LC

$$\frac{1}{2L_{\rm LC}}\frac{\left[\varphi_{\rm LC}^{(1)}\right]^2}{2} = \frac{1}{4}\hbar\omega_{\rm LC}, \tag{48}$$

in terms of the zero-point fluctuations $\varphi_{\rm LC}^{(1)}$ of the magnetic flux, we can directly estimate $\varphi_{\rm LC}^{(1)}$ in terms of circuit parameters, and then write the (operator-valued) magnetic flux threaded through the SQUID,

$$\delta\hat{\phi} = \frac{M}{L_{\rm LC}}\varphi_{\rm LC}^{(1)}\left(\frac{\hat{b}+\hat{b}^\dagger}{\sqrt{2}}\right) \tag{49}$$

in terms of the creation and destruction operators for the LC harmonic oscillator, $\hat{b}$ and $\hat{b}^\dagger$ in our notation.

Inserting this expression into the one for the effective length (47) and, this latter into the standard effective time-dependent Hamiltonian for the DCE emission in a cavity of average length x^o [57],

$$H_{\rm DCE}(t) = -\hbar\omega_a\frac{\delta x(t)}{2x^o}(\hat{a}+\hat{a}^\dagger)^2 \tag{50}$$

and promoting the position $\delta x(t)$ to an operator, one gets to an effective coupling Hamiltonian between the LC circuit and the (lowest) cavity mode in the desired form (3), with a coupling constant

$$\hbar\omega_c = \frac{\hbar\omega_a}{4\sqrt{2}\pi}\frac{M}{L_{\rm LC}}\frac{\omega_a}{I_J^o Z_{\rm wg}}\sqrt{\hbar\omega_{\rm LC}L_{\rm LC}}\,\frac{\sin(\pi\phi/\Phi_0)}{\cos^2(\pi\phi/\Phi_0)}. \tag{51}$$

Here we have considered the lowest mode of the waveguide with $\omega_a \approx \pi v/x^o$. Furthermore, $\omega_{\rm LC}$ is the frequency of the LC circuit (ω_b in the rest of the article), $v = \sqrt{\ell_{\rm wg}c_{\rm wg}}$ and $Z_{\rm wg} \equiv \sqrt{\ell_{\rm wg}/c_{\rm wg}}$ are, respectively, the velocity and the impedance of the waveguide mode in terms of the impedance $\ell_{\rm wg}$ and capacitance $c_{\rm wg}$ for unit length, and $I_J^o = 2\pi E_J^o/\Phi_0$ is the critical current of each Josephson junction forming the SQUID. A derivation of this same result starting from a more extended Lagrangian theory for the analog system is reported in the Appendix.

Plugging into this formula typical values for the SQUID device inspired from the experiment [54], namely an operating frequency $\omega_a/(2\pi) \approx 5$ GHz, an average cavity length of the order of a wavelength (in the waveguide) $x^o \approx 2\pi v/\omega_a$, a critical current $I_J^o \approx 1.25\ \mu$A, an impedance $Z_{\rm wg} \approx 55\ \Omega$, an inductance $L_{\rm LC} \approx 0.1$ nH (of the order of the kinetic inductance of the Josephson junction), a flux concatenation ratio $M/L_{\rm LC} = 0.1$, and a trigonometric factor of order 1, one obtains a value for $\hbar\omega_c$ in the order of a few 10^4 Hz. Given state-of-the-art values of the linewidths of superconductor-based oscillators in the tens of kHz range [63], this value for $\hbar\omega_c$ is very promising in view of experimental observation of the dynamical Casimir-induced damping of the LC circuit oscillations, as well as of the dynamical Casimir-induced periodic exchange of energy between the LC circuit and the coplanar cavity. From a physical standpoint, the strong value of the analog optomechanical coupling can be understood in terms of the very light mass that the LC circuit displays when viewed as an (analog) mechanical oscillator.

Finally, it is important to note that the LC circuit can be straightforwardly driven and/or monitored just by coupling it to an external circuit as shown in Fig. 6. This provides the experimental access needed to implement both the free evolution and the driven-dissipative steady-state schemes discussed in the previous section.

VI. CONCLUSIONS

In this work we have theoretically studied a simplest system where the backreaction effect of quantum fluctuations of the electromagnetic field onto a mechanically moving neutral object can be investigated. An optical cavity closed by a freely moving mirror attached to a spring is considered. The mechanical motion of the mirror is responsible for the conversion of zero-point quantum fluctuations of the electromagnetic field into real cavity photons via the dynamical Casimir effect, which then leak out of the cavity and can be observed as propagating radiation. In return, the dynamical Casimir photons exert a friction force on the moving mirror that damps its motion. This quantum friction effect is studied in two most remarkable configurations.

When no other external mechanical force is applied onto the mirror and the optomechanical coupling is relatively weak, the mirror motion performs periodic ring-down oscillations that are slowly damped out. The backreaction appears as an additional contribution to the damping rate on top of standard friction. Since dynamical Casimir emission is strongest when the mechanical oscillations are on resonance with twice the cavity frequency, the two contributions to damping can be disentangled by looking at the variation of the mechanical damping rate as a function of the cavity frequency. As first predicted in [37], for strong values of the optomechanical coupling, the monotonic decay of the ring-down oscillations is replaced by a periodic exchange of energy between the mechanical and optical degrees of freedom in a sort of dynamical Casimir-induced two-photon Rabi oscillations.

When a periodically oscillating external force is applied to the mirror, the system is able to reach at long times a stationary state characterized by periodic oscillations of the mirror and a continuous emission of dynamical Casimir

photons. In particular, we have shown how the properties of the backreaction force can be extracted from the dependence of the mechanical oscillation amplitude on the frequency of the applied force. For weak optomechanical couplings, this response shows a single yet broadened peak whose linewidth carries an additional contribution from the backreaction effect. For stronger couplings, the peak is replaced by a doublet whose splitting corresponds to the frequency of the periodic energy exchange between the mechanical and optical degrees of freedom.

While our study identified unambiguous signatures of the backreaction effect that could be used in experiments with standard optomechanical devices based on macro- or mesoscopic mechanically moving mirrors, the quantitatively weak magnitude of the predicted effects makes their actual experimental measurement a very challenging task. In the last part of our work, we have therefore investigated the observability of the backreaction effect in analog models based on circuit-QED systems. Taking inspiration from the device proposed in [51,52] and recently used in [54] for the observation of an analog of the dynamical Casimir effect, we propose a configuration where the massive, mechanically moving mirror is replaced by a SQUID element magnetically coupled to an independently evolving LC circuit. In such a system, the ring-down oscillations can be monitored by following in time the evolution of the oscillating current in the LC circuit. The response to the external force can be studied by sending an external monochromatic field onto the LC circuit and looking either at its current response or at the energy that is absorbed from the external field. The actual values of the system parameters that emerge from our simple modeling are extremely promising in view of experimental detection of the effect in state-of-the-art samples.

While the friction force of the dynamical Casimir effect onto the moving mirror is the simplest example of backreaction effect of quantum fluctuations onto their environment, the next theoretical steps will attack the far more difficult case of the backreaction of Hawking radiation onto a black hole horizon. Schemes to study this physics in analog models based on condensed matter or optical systems are being explored, with special attention to unveiling analogies and differences with the late-time evaporation of astrophysical black holes.

ACKNOWLEDGMENTS

We thank Andrea Vinante for helpful discussions on the experimental setups with superconducting circuits. This work was supported by Julian Schwinger foundation, Grant No. JSF-16-12-0001. Funding from Provincia Autonoma di Trento and from the EU-FET-Open Grant MIR-BOSE Project No.737017 is also acknowledged.

APPENDIX: LAGRANGIAN FORMULATION OF THE LC-SQUID-CPW SYSTEM

The following derivation is an extension of the Lagrangian formulation developed in [52], to the case in which the drive on the SQUID represents a dynamical degree-of-freedom for the system. Without affecting the generality of the following arguments, we assume the drive provided by a simple LC circuit which is magnetically coupled to the SQUID. Other devices could have been considered to the same aim, such as another CPW, or any other electronic circuit which can be magnetically coupled to the SQUID.

For convenience, we start by writing the Lagrangian for the lumped-element model of the circuit depicted in Fig. 7, and take the continuum limit after we calculate the equation of motion for the discrete degrees of freedom. Such a Lagrangian can be written as

$$\mathcal{L} = \mathcal{L}_{\rm CPW} + \mathcal{L}_{\rm SQUID} + \mathcal{L}_{\rm LC}, \tag{A1}$$

where

$$\mathcal{L}_{\rm CPW} = \sum_{n=1}^{N-1}\left[\frac{1}{2}\Delta x\, c_{\rm wg}\,\dot{\Phi}_n^2 - \frac{1}{2}\frac{(\Phi_{n+1}-\Phi_n)^2}{\Delta x\,\ell_{\rm wg}}\right], \tag{A2}$$

$$\mathcal{L}_{\rm SQUID} = \sum_{j=1,2}\left[\frac{1}{2}C_{J,j}(\dot{\Phi}_{J,j})^2 + E_{J,j}\cos\left(2\pi\frac{\Phi_{J,j}}{\Phi_0}\right)\right], \tag{A3}$$

$$\mathcal{L}_{\rm LC} = \frac{1}{2}C_{\rm LC}\dot{\Phi}_{\rm LC}^2 - \frac{1}{2L_{\rm LC}}\Phi_{\rm LC}^2 \tag{A4}$$

are the Lagrangian for the CPW, the SQUID, and the LC resonator, respectively. Here we defined the flux quantum $\Phi_0 \equiv \pi\hbar/e$ (e is the electron charge), the capacitance $c_{\rm wg}$ and inductance $\ell_{\rm wg}$ densities in the CPW, the capacitance $C_{\rm LC}$ and inductance $L_{\rm LC}$, respectively, for the capacitor and inductor in the LC resonator, as well as the capacitance $C_{J,j}$ and the Josephson energy $E_{J,j} = \hbar I_{c,j}/2e$ of the jth junction in the SQUID loop, characterized by the critical current $I_{c,j}$. We wrote the Lagrangian in Eqs. (A2)–(A4) by assuming the node fluxes as generalized coordinates, which are defined as the time integral of the local voltage V_j,

$$\Phi_j(t) \equiv \int^t d\tau V_j(\tau). \tag{A5}$$

Here $j = 1, 2, \ldots, N$ denote the (discrete) degrees-of-freedom of the CPW, while $j = \mathrm{LC}$ refers to the flux and the voltage across the LC resonator. We dropped from $\mathcal{L}_{\rm SQUID}$ a term $(LI^2)_{\rm SQUID}/2$, accounting for the magnetic energy stored in the SQUID because of the current $I_{\rm SQUID}$ circulating in the loop. In other terms, we assumed the size of the SQUID loop small enough so that its self-inductance $L_{\rm SQUID}$ is negligible compared to the Josephson inductances $L_{J,j} = (\Phi_0/2\pi)^2/E_{J,j}$. Given these assumptions, the fluxes $\Phi_{J,j}$ across the junctions can be directly related to the external flux piercing the loop as $\Phi_{J,1} - \Phi_{J,2} = \phi$, so that the SQUID can be described by the single degree of freedom $\Phi_J = (\Phi_{J,1} + \Phi_{J,2})/2$. As a consequence, the SQUID behaves as a single Josephson junction described, in the simpler case of a perfectly symmetric junction characterized by the values $C_{J,1} = C_{J,2} = C_J^o/2$ and $E_{J,1} = E_{J,1} = E_J^o$, by the effective Lagrangian

$$\mathcal{L}_{\rm SQUID} = \frac{1}{2}C_J^o\dot{\Phi}_J^2 + E_J(\phi)\cos\left(2\pi\frac{\Phi_J}{\Phi_0}\right). \tag{A6}$$

Here we indicated by $E_J(\phi) = 2E_J^o|\cos(\pi\frac{\phi}{\Phi_0})|$ the energy stored in the SQUID, which is a nonlinear function of the external flux piercing the flux. We work in the limit in which the plasma frequency $\omega_S^2 = (2\pi/\Phi_0)^2(2E_J^o/C_J^o)$ of the SQUID

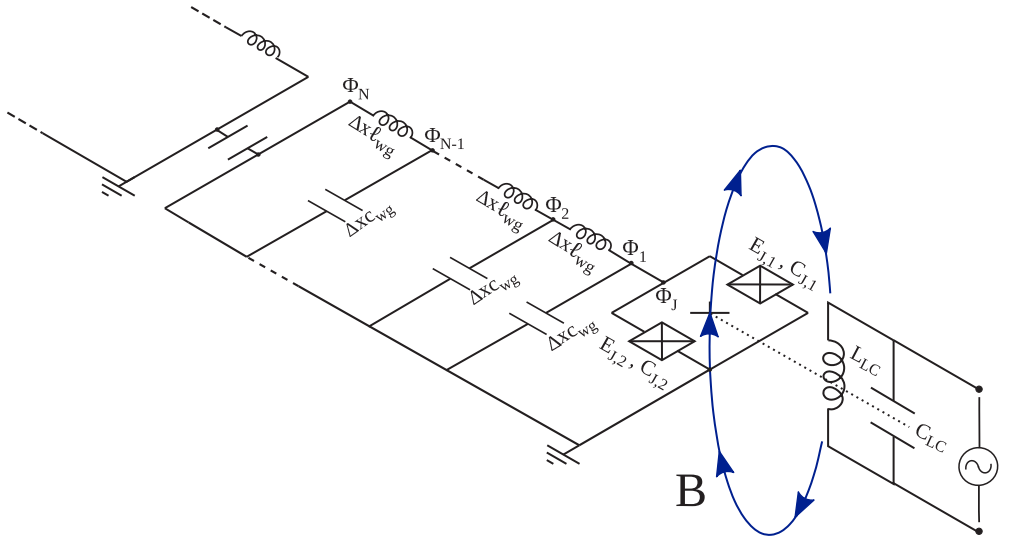

FIG. 7. Discrete model of the CPW magnetically coupled with the LC circuit.

far exceed the other characteristic frequencies in the circuit. In this regime, the oscillations of the phase across the SQUID are small, that is $\Phi_J/\Phi_0 \ll 1$. Furthermore, we consider the external magnetic field piercing the SQUID to perform small oscillations around a bias value ϕ_b, and we call $\delta\phi$ the amplitude of these oscillations, which are driven by the LC resonator magnetically coupled with its loop. With these assumptions we can approximate the SQUID Lagrangian by using the expansions

$$\cos\left(2\pi\frac{\Phi_J}{\Phi_0}\right) \approx 1 - \left(\frac{2\pi}{\Phi_0}\right)^2 \frac{\Phi_J^2}{2}, \tag{A7}$$

$$\begin{aligned} E_J(\phi) &= 2E_J^o\left|\cos\left(\pi\frac{\phi}{\Phi_0}\right)\right| = 2E_J^o\left|\cos\left(\pi\frac{\phi_b+\delta\phi}{\Phi_0}\right)\right| \\ &\approx 2E_J^o\cos\left(\pi\frac{\phi_b}{\Phi_0}\right) - 2E_J^o\sin\left(\pi\frac{\phi_b}{\Phi_0}\right)\left(\pi\frac{\delta\phi}{\Phi_0}\right). \end{aligned} \tag{A8}$$

In the third line in Eq. (A8) we assumed the amplitude of the oscillations $\delta\phi$ small enough so that the overall flux piercing the SQUID does not change sign. For the sake of brevity, we label in what follows $\varphi_b = \pi\phi_b/\Phi_0$, and write $\delta\phi = \chi\Phi_{\rm LC}$, being $\chi \equiv M/L_{\rm LC}$, where M is the mutual inductance between the LC and the SQUID and $\Phi_{\rm LC}$ is the flux through the LC circuit. Under these assumptions, the Lagrangian for the SQUID-LC subsystem can be written in the form

$$\mathcal{L}_{\rm SQUID} + \mathcal{L}_{\rm LC} = \mathcal{L}'_{\rm SQUID} + \mathcal{L}'_{\rm LC} + \mathcal{L}_{\rm int}, \tag{A9}$$

with

$$\mathcal{L}'_{\rm SQUID} = \frac{1}{2}C_J^o\dot{\Phi}_J^2 - E_J^o\left(\frac{2\pi}{\Phi_0}\right)^2\cos\varphi_b\Phi_J^2, \tag{A10}$$

$$\mathcal{L}'_{\rm LC} = \frac{1}{2}C_{\rm LC}\dot{\Phi}_{\rm LC}^2 - \frac{1}{2L_{\rm LC}}\Phi_{\rm LC}^2 - \chi E_J^o\left(\frac{2\pi}{\Phi_0}\right)\sin\varphi_b\Phi_{\rm LC}, \tag{A11}$$

$$\mathcal{L}'_{\rm int} = \chi\frac{E_J^o}{2}\left(\frac{2\pi}{\Phi_0}\right)^3\sin\varphi_b\Phi_J^2\Phi_{\rm LC}. \tag{A12}$$

The Lagrangian in Eqs. (A10) and (A11) describes the free evolution of the SQUID and the LC resonator, respectively. There we notice the presence of a term linear in the flux $\Phi_{\rm LC}$, which accounts for a shift of the equilibrium position of the oscillator, due to its coupling with the SQUID. The Lagrangian in Eq. (A12) is instead cubic in the products between the flux Φ_J across the junction and the flux $\Phi_{\rm LC}$ across the inductance of the LC, and is responsible for a coupling between the two devices. In terms of Eqs. (A2) and (A10)–(A12), the Lagrangian for the full circuit can thus be written as

$$\mathcal{L} = \mathcal{L}_{\rm CPW} + \mathcal{L}'_{\rm SQUID} + \mathcal{L}'_{\rm LC} + \mathcal{L}'_{\rm int}. \tag{A13}$$

Equations of motion

a. Radiation field

Basing on the effective Lagrangian in Eq. (A13), we determine here the equation of motion for the electromagnetic field. In the bulk region of the medium, in the continuum limit $\Delta x \to 0$, the field satisfies the wave equation

$$\frac{\partial^2\Phi}{\partial t^2} - v^2\frac{\partial^2\Phi}{\partial x^2} = 0, \tag{A14}$$

where $v = 1/\sqrt{c_{\rm wg}\ell_{\rm wg}}$ is the velocity of light in the CPW. Beside this, we need to pose opportune boundary conditions (BCs) to the field. On the side opposite to the SQUID, that is at $x = -L$, such a BC is determined by the fact that the CPW is open and the current $I_{\rm wg}$ need to be zero. Here the current is written in terms of the flux on the N and $N-1$ node as $(\Phi_N - \Phi_{N-1}) = I_{\rm wg}(\ell_{\rm wg}\Delta x)$, from which follows in the continuum limit $I_{\rm wg} = -\partial\Phi/(\ell_{\rm wg}\partial x)$. This yields the first BC

$$\frac{\partial\Phi(t,-L)}{\partial x} = 0. \tag{A15}$$

On the SQUID side instead, posing a BC means fixing the value of $\Phi(0,t)$, which corresponds to Φ_1 in the discretized version of the Lagrangian in Eq. (A2). It is important here to note that, in the model analyzed, Φ_1 is not only a BC for the

field, but it is a true dynamical quantity for the system. To determine the corresponding equation of motion, we notice that Φ_1 coincides with the flux Φ_J across the junctions (see Fig. 7). By posing $\Phi_J = \Phi_1$, and minimizing the Lagrangian in Eq. (A13) with respect to variations in Φ_1, we obtain, again in the continuum limit,

$$C_J^o \ddot{\Phi}(t,0) + \frac{1}{\ell_{\rm wg}} \frac{\partial \Phi}{\partial x}(t,0) + 2E_J^o \left(\frac{2\pi}{\Phi_0}\right)^2 \cos\varphi_b \, \Phi(t,0) - E_J^o \left(\frac{2\pi}{\Phi_0}\right)^3 \chi \sin\varphi_b \, \Phi(t,0)\Phi_{\rm LC} = 0. \tag{A16}$$

Since we work in the regime $\omega^2 \ll \omega_S^2$, the first term in Eq. (A16) can be neglected, which reduces to

$$\Phi(t,0) + \frac{\partial \Phi}{\partial x}(t,0)\delta L_{\rm eff} = 0. \tag{A17}$$

Here we defined the effective variation of the CPW length

$$\delta L_{\rm eff} = \frac{1}{2E_J^o \ell_{\rm wg} \cos\varphi_b} \left(\frac{\Phi_0}{2\pi}\right)^2 \frac{1}{(1 - \pi\chi \tan\varphi_b \Phi_{\rm LC}/\Phi_0)}. \tag{A18}$$

To first order in $\Phi_{\rm LC}/\Phi_0$, such an effective length is given by the sum of the two contributions

$$\delta L_{\rm eff} = \delta L_{\rm eff}^{\phi_b} + \delta L_{\rm eff}^{\delta\phi}. \tag{A19}$$

Here

$$\delta L_{\rm eff}^{\phi_b} \equiv \frac{1}{\cos\varphi_b} \frac{L_J}{\ell_{\rm wg}} \tag{A20}$$

is an effective length experienced by the CPW as an effect of the bias component ϕ_b of the magnetic flux concatenated with the SQUID, while

$$\delta L_{\rm eff}^{\delta\phi} = \frac{\Phi_{\rm LC}}{R}, \tag{A21}$$

with

$$R = \left(\tan\varphi_b \pi \chi \delta L_{\rm eff}^{\phi_b}\right)^{-1} \Phi_0 \tag{A22}$$

is an effective length induced by the drive. In Eq. (A20) we introduced the characteristic inductance of the SQUID $L_J = (\Phi_0/2\pi)^2/(2E_J^o)$. For convenience we shift in what follows the origin of the x coordinate by L, and rewrite the BCs obtained above as

$$\frac{\partial \Phi(t,0)}{\partial x} = 0, \tag{A23}$$

$$\Phi(t,L) + \frac{\partial \Phi}{\partial x}(t,L)\delta L_{\rm eff} = 0. \tag{A24}$$

The former is satisfied by choosing field modes of the form $\cos(k_n x)$, while the latter sets the allowed values of the wave vector κ_n, which need to satisfy the following relation:

$$(\kappa_n \delta L_{\rm eff}) \tan(\kappa_n L) = 1. \tag{A25}$$

In the limit $\kappa_n \delta L_{\rm eff} \ll 1$, the BC at $x = L$ can be simplified as

$$\Phi(t,d) = 0, \tag{A26}$$

with $d = L + \delta L_{\rm eff}$ the total effective length of the CPW. From the BC written in this form we find the allowed wave vectors $\kappa_n = (2n+1)\pi/2d(t)$. The (normalized) basis functions, at the generic time instant t, can thus be written as

$$\varphi_n(x) = \sqrt{\frac{2}{d(t)}} \cos(\kappa_n x), \tag{A27}$$

in terms of which the field in the CPW can be expanded as $\Phi(t,x) = \sum_n Q_n(t)\varphi_n(x)$, with $Q_n(t)$ the coefficients of the expansion, having the units [flux] × [length]$^{1/2}$. Upon substitution of Eq. (A27) into the equation of motion in Eq. (A14), we obtain the equation of motion for the Q_n,

$$\ddot{Q}_n + \omega_n^2 Q_n - 2\frac{\dot{d}}{d}\sum_k \dot{Q}_n g_{nk} - \left(\frac{\ddot{d}d - \dot{d}^2}{d^2}\right)\sum_k Q_k g_{nk} - \frac{\dot{d}^2}{d^2}\sum_{k,j} Q_k g_{kj} g_{nj} = 0, \tag{A28}$$

with the coefficients

$$g_{nk} = \begin{cases} \frac{(-1)^{n+k}}{2} \frac{(1+2k)(1+2n)}{k(k+1-n(n+1))} & \text{if } n \neq k, \\ 0 & \text{if } n = k. \end{cases} \tag{A29}$$

b. The LC resonator and its effective mass

In the previous section we derived the equation of motion for the field in the CPW. Since one of the BCs is nonstationary, we expanded the field in the instantaneous basis of eigenmodes $\{\varphi_n(x)\}$, and wrote the equation describing the time evolution for the coefficients Q_k of such an expansion. This procedure is not new in literature, but has been pursued in order to calculate the particle production from DCE or in cosmological scenarios as expanding universes [1,64,65]. What is different in the problem we study is that we consider the BC, which is the LC resonator in our case, as a truly dynamical object. In this section we study its dynamics, and derive the equation that describes the evolution in time of the effective length $d(t)$ of the CPW. The ultimate aim of this procedure is to introduce the effective mass for the BC, and provide an estimate for its value.

We start from the Euler-Lagrange equation for the LC resonator, which can be obtained directly from the Lagrangian in Eq. (A9). This has the form

$$\ddot{\Phi}_{\rm LC} + \omega_{\rm LC}^2 \Phi_{\rm LC} + \left(\frac{\Phi_0}{2\pi}\right)\frac{\chi}{2L_J C_{\rm LC}} \sin\varphi_b - \left(\frac{2\pi}{\Phi_0}\right)\frac{\chi}{4L_J C_{\rm LC}} \sin\varphi_b \, \Phi^2(t,L) = 0. \tag{A30}$$

The value of the field $\Phi(t,L)$ at $x = L$ is obtained from the BC in Eq. (A26),

$$\Phi(t,L) = -\frac{\partial\phi}{\partial x}[d(t)][d(t) - L] = \sqrt{\frac{2}{d}}\left(\sum_n (-1)^n \kappa_n Q_n\right)[d(t) - L], \tag{A31}$$

where we used here the expansion $\Phi(t,x)=\sum_n Q_n(t)\varphi_n(x)$, along with the definition in Eq. (A27) for the field eigenmodes. Upon substitution of Eq. (A31) into Eq. (A30) we can write the equation for the LC resonator as

$$\ddot{\Phi}_{\rm LC}+\omega_{\rm LC}^2\Phi_{\rm LC}+\left(\frac{\Phi_0}{2\pi}\right)\frac{\chi}{2L_JC_{\rm LC}}\sin\varphi_b\left[1-\left(\frac{2\pi}{\Phi_0}\right)^2\frac{(d-L)^2}{d}\left(\sum_{n,k}(-1)^{n+k}Q_nQ_k\kappa_n\kappa_k\right)\right]=0. \tag{A32}$$

In writing Eq. (A32) we neglected a correction to the LC frequency, induced by the electromagnetic field in the CPW. In order to make a connection with the optomechanical problem discussed in the previous sections, we write this equation in standard mechanical units and define an effective mass for the LC oscillator. To this aim we start from the free Lagrangian

$$\mathcal{L}_{\rm LC}=\frac{1}{2}C_{\rm LC}\dot{\Phi}_{\rm LC}^2-\frac{1}{2L_{\rm LC}}\Phi_{\rm LC}^2, \tag{A33}$$

and write it in terms of the effective length d defined above. By using Eq. (A21), this takes the form

$$\mathcal{L}_{\rm LC}=\frac{1}{2}C_{\rm LC}R^2\dot{d}^2-\frac{1}{2L_{\rm LC}}R^2\left[d-\left(L+\delta L_{\rm eff}^{\phi_b}\right)\right]^2. \tag{A34}$$

The momentum conjugate to the effective length d is

$$p=\frac{\partial\mathcal{L}_{\rm LC}}{\partial\dot{d}}=C_{\rm LC}R^2\dot{d}, \tag{A35}$$

and allows us to identify the effective mass $m=R^2C_{\rm LC}$. Considering typical values for the physical parameters of the system, such an effective mass can take values of the order

$$m=C_{\rm LC}R^2=C_{\rm LC}\left(\frac{\cos\varphi_b}{\tan\varphi_b}\frac{\ell_{\rm wg}}{L_J}\frac{\Phi_0}{\pi\chi}\right)^2\sim 10^{-30}\ \text{kg}. \tag{A36}$$

In terms of these quantities, Eq. (A32) can be rewritten as

$$m\ddot{d}+m\omega_{\rm LC}^2(d-L_{\rm eq})-\frac{1}{d}\sum_{kn}(-1)^{n+k}\tilde{Q}_n\tilde{Q}_k\omega_n\omega_k=0. \tag{A37}$$

Here we defined the quantities

$$\tilde{Q}_n\equiv\left(\frac{2\pi}{\Phi_0}\right)\delta L_{\rm eff}^{\phi_b}\left(\frac{ma}{v^2}\right)^{1/2}Q_n, \tag{A38}$$

$$L_{\rm eq}\equiv L+\delta L_{\rm eff}^{\phi_b}-\frac{a}{\omega_{\rm LC}^2}, \tag{A39}$$

$$a\equiv\frac{R\Phi_0}{2\pi}\frac{\chi}{2L_Jm}\sin\varphi_b, \tag{A40}$$

and used the zeroth order approximation

$$\frac{(d-L)^2}{d}\approx\frac{\left(\delta L_{\rm eff}^{\phi_b}\right)^2}{d}. \tag{A41}$$

The coefficients $\tilde{Q}_n$ have here the units [length] × [mass]$^{1/2}$, and Eq. (A37) is equivalent to the equation of motion of a mirror interacting with an electromagnetic field via its radiation pressure. We do not go through the quantization procedure for this theory. It is laborious and already addressed in [57]. For our purposes it is sufficient to remember that, in the regime of small oscillations of the mirror around its equilibrium position, the quantized theory leads to the Hamiltonian we used in Eq. (3) to describe the interaction. By taking advantage of this analogy, the value of the effective coupling constant can be calculated by using the definition in Eq. (4) given in Sec. II (with $\omega_{\rm LC}$ in place of ω_b). Given the expression for the effective mass in Eq. (A36), this reproduces the result in Eq. (51) of the main text.

[1] N. D. Birrell and P. C. W. Davies, *Quantum Fields in Curved Space*, Cambridge Monographs on Mathematical Physics (Cambridge University Press, Cambridge, 1984).

[2] S. W. Hawking, Particle creation by black holes, Commun. Math. Phys **43**, 199 (1975).

[3] L. Parker, Quantized fields and particle creation in expanding universes. I, Phys. Rev. **183**, 1057 (1969).

[4] L. Parker, Quantized fields and particle creation in expanding universes. II, Phys. Rev. D **3**, 346 (1971).

[5] S. A. Fulling and P. C. W. Davies, Radiation from a moving mirror in two dimensional space-time: Conformal anomaly, Proc. R. Soc. London Ser. A **348**, 393 (1976).

[6] V. V. Dodonov, Current status of the dynamical Casimir effect, Phys. Scr. **82**, 038105 (2010).

[7] A. Lambrecht, Electromagnetic pulses from an oscillating high-finesse cavity: Possible signatures for dynamic Casimir effect experiments, J. Opt. B **7**, S3 (2005).

[8] Y. B. Zeldovich and A. A. Starobinsky, Particle production and vacuum polarization in an anisotropic gravitational field, Zh. Eksp. Teor. Fiz. **61**, 2161 (1971) [Sov. Phys. JETP **34**, 1159 (1972)].

[9] B. L. Hu, S. A. Fulling, and L. Parker, Quantized scalar fields in a closed anisotropic universe, Phys. Rev. D **8**, 2377 (1973).

[10] L. Parker and S. A. Fulling, Quantized matter fields and the avoidance of singularities in general relativity, Phys. Rev. D **7**, 2357 (1973).

[11] B. L. Hu, Scalar waves in the mixmaster universe. I. The Helmholtz equation in a fixed background, Phys. Rev. D **8**, 1048 (1973).

[12] B. L. Hu, Scalar waves in the mixmaster universe. II. Particle creation, Phys. Rev. D **9**, 3263 (1974).

[13] J. B. Hartle, Effective-Potential Approach to Graviton Production in the Early Universe, Phys. Rev. Lett. **39**, 1373 (1977).

[14] B. L. Hu and L. Parker, Anisotropy damping through quantum effects in the early universe, Phys. Rev. D **17**, 933 (1978).

[15] M. V. Fischetti, J. B. Hartle, and B. L. Hu, Quantum effects in the early universe. I. Influence of trace anomalies on homogeneous, isotropic, classical geometries, Phys. Rev. D **20**, 1757 (1979).

[16] J. B. Hartle and B. L. Hu, Quantum effects in the early universe. II. Effective action for scalar fields in homogeneous cosmologies with small anisotropy, Phys. Rev. D **20**, 1772 (1979).

[17] J. B. Hartle and B. L. Hu, Quantum effects in the early universe. III. Dissipation of anisotropy by scalar particle production, Phys. Rev. D **21**, 2756 (1980).

[18] A. Shaw, D. Biswas, B. Modak, and S. Biswas, Particle production, back reaction and singularity avoidance, Pramana **52**, 1 (1999).

[19] J. D. Bekenstein, Black holes and the second law, Lett. Nuovo Cimento **4**, 737 (1972).

[20] J. M. Bardeen, B. Carter, and S. W. Hawking, The four laws of black hole mechanics, Commun. Math. Phys. **31**, 161 (1973).

[21] J. D. Bekenstein, Black holes and entropy, Phys. Rev. D **7**, 2333 (1973).

[22] D. N. Page, Hawking radiation and black hole thermodynamics, New J. Phys. **7**, 203 (2005).

[23] R. M. Wald, The thermodynamics of black holes, Living Rev. Relativity **4**, 6 (2001).

[24] A. Fabbri and J. Navarro-Salas, *Modeling Black Hole Evaporation* (Imperial College Press, London, 2005).

[25] M. Kardar and R. Golestanian, The "friction" of vacuum, and other fluctuation-induced forces, Rev. Mod. Phys. **71**, 1233 (1999).

[26] K. Oku and Y. Tsuchida, Back-reaction in the moving mirror effects, Prog. Theor. Phys. **62**, 1756 (1979).

[27] A. Xuereb, P. Domokos, J. Asbóth, P. Horak, and T. Freegarde, Scattering theory of cooling and heating in optomechanical systems, Phys. Rev. A **79**, 053810 (2009).

[28] C. R. Galley, R. O. Behunin, and B. L. Hu, Oscillator-field model of moving mirrors in quantum optomechanics, Phys. Rev. A **87**, 043832 (2013).

[29] K. Sinha, S.-Y. Lin, and B. L. Hu, Mirror-field entanglement in a microscopic model for quantum optomechanics, Phys. Rev. A **92**, 023852 (2015).

[30] A. Lambrecht, M.-T. Jaekel, and S. Reynaud, Motion Induced Radiation from a Vibrating Cavity, Phys. Rev. Lett. **77**, 615 (1996).

[31] W.-J. Kim, J. H. Brownell, and R. Onofrio, Detectability of Dissipative Motion in Quantum Vacuum via Superradiance, Phys. Rev. Lett. **96**, 200402 (2006).

[32] G. Barton and C. Eberlein, On quantum radiation from a moving body with finite refractive index, Ann. Phys. **227**, 222 (1993).

[33] M. Aspelmeyer, T. J. Kippenberg, and F. Marquardt, Cavity optomechanics, Rev. Mod. Phys. **86**, 1391 (2014).

[34] A. D. O'Connell, M. Hofheinz, M. Ansmann, R. C. Bialczak, M. Lenander, E. Lucero, M. Neeley, D. Sank, H. Wang, M. Weides *et al.*, Quantum ground state and single-phonon control of a mechanical resonator, Nature (London) **464**, 697 (2010).

[35] Y. Chu, P. Kharel, W. H. Renninger, L. D. Burkhart, L. Frunzio, P. T. Rakich, and R. J. Schoelkopf, Quantum acoustics with superconducting qubits, Science **358**, 199 (2017).

[36] P. Kharel, Y. Chu, M. Power, W. H. Renninger, R. J. Schoelkopf, and P. T. Rakich, Ultra-high-Q phononic resonators on-chip at cryogenic temperatures, APL Photon. **3**, 066101 (2018).

[37] V. Macrì, A. Ridolfo, O. Di Stefano, A. F. Kockum, F. Nori, and S. Savasta, Nonperturbative Dynamical Casimir Effect in Optomechanical Systems: Vacuum Casimir-Rabi Splittings, Phys. Rev. X **8**, 011031 (2018).

[38] W. Qin, V. Macrì, A. Miranowicz, S. Savasta, and F. Nori, Experimentally feasible dynamical casimir effect in parametrically amplified cavity optomechanics, arXiv:1902.04216.

[39] W. G. Unruh, Experimental Black-Hole Evaporation? Phys. Rev. Lett. **46**, 1351 (1981).

[40] C. Barcelo, S. Liberati, and M. Visser, Analogue gravity, Living Rev. Relativity **14**, 3 (2011).

[41] I. Carusotto, S. Fagnocchi, A. Recati, R. Balbinot, and A. Fabbri, Numerical observation of Hawking radiation from acoustic black holes in atomic Bose–Einstein condensates, New J. Phys. **10**, 103001 (2008).

[42] J. Steinhauer, Observation of quantum Hawking radiation and its entanglement in an analogue black hole, Nat. Phys. **12**, 959 (2016).

[43] P. D. Nation, M. P. Blencowe, A. J. Rimberg, and E. Buks, Analogue Hawking Radiation in a dc-SQUID Array Transmission Line, Phys. Rev. Lett. **103**, 087004 (2009).

[44] Yu. E. Lozovik, V. G. Tsvetus, and E. A. Vinogradov, Femtosecond parametric excitation of electromagnetic field in a cavity, Pis'ma Zh. Éksp. Teor. Fiz. **61**, 711 (1995) [JETP Lett. **61**, 723 (1995)].

[45] E. Yablonovitch, Accelerating Reference Frame for Electromagnetic Waves in a Rapidly Growing Plasma: Unruh-Davies-Fulling-DeWitt Radiation and the Nonadiabatic Casimir Effect, Phys. Rev. Lett. **62**, 1742 (1989).

[46] C. Braggio, G. Bressi, G. Carugno, C. Del Noce, G. Galeazzi, A. Lombardi, A. Palmieri, G. Ruoso, and D. Zanello, A novel experimental approach for the detection of the dynamical Casimir effect, Europhys. Lett. **70**, 754 (2005).

[47] I. Carusotto, R. Balbinot, A. Fabbri, and A. Recati, Density correlations and analog dynamical Casimir emission of Bogoliubov phonons in modulated atomic Bose–Einstein condensates, Eur. Phys. J. D **56**, 391 (2010).

[48] J.-C. Jaskula, G. B. Partridge, M. Bonneau, R. Lopes, J. Ruaudel, D. Boiron, and C. I. Westbrook, Acoustic Analog to the Dynamical Casimir Effect in a Bose-Einstein Condensate, Phys. Rev. Lett. **109**, 220401 (2012).

[49] C.-L. Hung, V. Gurarie, and C. Chin, From cosmology to cold atoms: Observation of Sakharov oscillations in a quenched atomic superfluid, Science **341**, 1213 (2013).

[50] P. D. Nation, J. R. Johansson, M. P. Blencowe, and F. Nori, Colloquium: Stimulating uncertainty: Amplifying the quantum vacuum with superconducting circuits, Rev. Mod. Phys. **84**, 1 (2012).

[51] J. R. Johansson, G. Johansson, C. M. Wilson, and F. Nori, Dynamical Casimir Effect in a Superconducting Coplanar Waveguide, Phys. Rev. Lett. **103**, 147003 (2009).

[52] J. R. Johansson, G. Johansson, C. M. Wilson, and F. Nori, Dynamical Casimir effect in superconducting microwave circuits, Phys. Rev. A **82**, 052509 (2010).

[53] S. De Liberato, D. Gerace, I. Carusotto, and C. Ciuti, Extracavity quantum vacuum radiation from a single qubit, Phys. Rev. A **80**, 053810 (2009).

[54] C. W. Wilson, G. Johansson, A. Pourkabirian, M. Simoen, J. R. Johansson, T. Duty, F. Nori, and P. Delsing, Observation of the dynamical Casimir effect in a superconducting circuit, Nature (London) **479**, 376 (2011).

[55] P. Lähteenmäki, G. S. Paraoanu, J. Hassel, and P. J. Hakonen, Dynamical Casimir effect in a Josephson metamaterial, Proc. Natl. Acad. Sci. **110**, 4234 (2013).

[56] I. Carusotto, S. De Liberato, D. Gerace, and C. Ciuti, Backreaction effects of quantum vacuum in cavity quantum electrodynamics, Phys. Rev. A **85**, 023805 (2012).

[57] C. K. Law, Interaction between a moving mirror and radiation pressure: A Hamiltonian formulation, Phys. Rev. A **51**, 2537 (1995).

[58] S. Butera and R. Passante, Field Fluctuations in a One-Dimensional Cavity with a Mobile Wall, Phys. Rev. Lett. **111**, 060403 (2013).

[59] C. Cohen-Tannoudji, J. Dupont-Roc, and G. Grynberg, *Atom-Photon Interactions: Basic Processes and Applications* (Wiley, Berlin, 1998).

[60] K Børkje and S M Girvin, Quantum optomechanics with a high-frequency dilational mode in thin dielectric membranes, New J. Phys. **14**, 085016 (2012).

[61] I. Carusotto and G. C. La Rocca, Two photon Rabi splitting and optical Stark effect in semiconductor microcavities, Phys. Rev. B **60**, 4907 (1999).

[62] C. M. Wilson, T. Duty, M. Sandberg, F. Persson, V. Shumeiko, and P. Delsing, Photon Generation in an Electromagnetic Cavity with a Time-Dependent Boundary, Phys. Rev. Lett. **105**, 233907 (2010).

[63] X. Gu, A. F. Kockum, A. Miranowicz, Y.-X. Liu, and F. Nori, Microwave photonics with superconducting quantum circuits, Phys. Rep. **718-719**, 1 (2017).

[64] M. Crocce, D. A. R. Dalvit, and F. D. Mazzitelli, Resonant photon creation in a three-dimensional oscillating cavity, Phys. Rev. A **64**, 013808 (2001).

[65] M. Crocce, D. A. R. Dalvit, and F. D. Mazzitelli, Quantum electromagnetic field in a three-dimensional oscillating cavity, Phys. Rev. A **66**, 033811 (2002).